# Reprogramming to recover youthful epigenetic information and restore vision

https://doi.org/10.1038/s41586-020-2975-4

Received: 31 July 2019

Accepted: 22 October 2020

Published online: 2 December 2020

Check for updates

Yuancheng Lu[1], Benedikt Brommer[2,3,11], Xiao Tian[1,11], Anitha Krishnan[3,4,11], Margarita Meer[5,6,11], Chen Wang[2,3], Daniel L. Vera[1], Qiurui Zeng[1], Doudou Yu[1], Michael S. Bonkowski[1], Jae-Hyun Yang[1], Songlin Zhou[2,3], Emma M. Hoffmann[3,4], Margarete M. Karg[3,4], Michael B. Schultz[1], Alice E. Kane[1], Noah Davidsohn[7], Ekaterina Korobkina[3,4], Karolina Chwalek[1], Luis A. Rajman[1], George M. Church[7], Konrad Hochedlinger[8], Vadim N. Gladyshev[5], Steve Horvath[9], Morgan E. Levine[6], Meredith S. Gregory-Ksander[3,4,12], Bruce R. Ksander[3,4,12], Zhigang He[2,3,12] & David A. Sinclair[1,10,12] ✉

Ageing is a degenerative process that leads to tissue dysfunction and death. A proposed cause of ageing is the accumulation of epigenetic noise that disrupts gene expression patterns, leading to decreases in tissue function and regenerative capacity[1–3]. Changes to DNA methylation patterns over time form the basis of ageing clocks[4], but whether older individuals retain the information needed to restore these patterns—and, if so, whether this could improve tissue function—is not known. Over time, the central nervous system (CNS) loses function and regenerative capacity[5–7]. Using the eye as a model CNS tissue, here we show that ectopic expression of *Oct4* (also known as *Pou5f1*), *Sox2* and *Klf4* genes (OSK) in mouse retinal ganglion cells restores youthful DNA methylation patterns and transcriptomes, promotes axon regeneration after injury, and reverses vision loss in a mouse model of glaucoma and in aged mice. The beneficial effects of OSK-induced reprogramming in axon regeneration and vision require the DNA demethylases TET1 and TET2. These data indicate that mammalian tissues retain a record of youthful epigenetic information—encoded in part by DNA methylation—that can be accessed to improve tissue function and promote regeneration in vivo.

The metaphor of the epigenetic landscape, which was first invoked to explain embryonic development[8], is increasingly being seen as relevant to the later stages of life[9]. Evidence from yeast and mammals supports an information theory of ageing[10,11], in which the loss of epigenetic information disrupts youthful gene expression patterns[1–3], leading to cellular dysfunction and senescence[12,13].

DNA methylation patterns are laid down during embryonic development to establish cell type and function. During ageing, for reasons that are currently unclear, these patterns change in ways that can be used to calculate DNA methylation age—a representation of biological age that can predict future health and lifespan[4]. In cell culture, the ectopic expression of the four Yamanaka transcription factors OCT4, SOX2, KLF4 and MYC (OSKM) can reprogram cultured somatic cells to become pluripotent stem cells[14]—a process that erases cellular identity and resets DNA methylation age[4,15]. In a premature-ageing mouse model of Hutchinson–Gilford progeria syndrome, cyclic transgene-mediated expression of the four genes encoding these transcription factors alleviates symptoms and extends lifespan, raising the possibility that OSKM might also counteract normal ageing[16]. The continuous expression of all four factors in mice, however, often induces teratomas[17–19] or is fatal within days[16], ostensibly due to tissue dysplasia[18].

Ageing is generally considered to be a unidirectional process, akin to an increase in entropy. However, living systems are open, not closed, and in some cases biological age can be fully reset, for example in 'immortal' jellyfish and through the cloning of animals by nuclear transfer. Having previously found evidence for epigenetic noise as an underlying cause of ageing[3,13], we wondered whether mammalian cells might retain a faithful copy of epigenetic information from earlier in life that could serve as instructions to reverse ageing[10].

## Reset of ageing signatures rather than identity

Our first goal was to find a way to reset the epigenome without erasing cell identity. Among the genes expressing the Yamanaka factors, *Myc*

[1]Department of Genetics, Blavatnik Institute, Paul F. Glenn Center for Biology of Aging Research, Harvard Medical School, Boston, MA, USA. [2]Department of Neurology, Boston Children's Hospital, Harvard Medical School, Boston, MA, USA. [3]Department of Ophthalmology, Harvard Medical School, Boston, MA, USA. [4]Schepens Eye Research Institute of Mass Eye and Ear, Harvard Medical School, Boston, MA, USA. [5]Division of Genetics, Department of Medicine, Brigham and Women's Hospital, Harvard Medical School, Boston, MA, USA. [6]Department of Pathology, Yale School of Medicine, New Haven, CT, USA. [7]Department of Genetics, Wyss Institute for Biologically Inspired Engineering, Harvard University, Boston, MA, USA. [8]Department of Molecular Biology, Cancer Center and Center for Regenerative Medicine, Massachusetts General Hospital, Boston, MA, USA. [9]Department of Human Genetics, David Geffen School of Medicine, University of California Los Angeles, Los Angeles, CA, USA. [10]Laboratory for Ageing Research, Department of Pharmacology, School of Medical Sciences, The University of New South Wales, Sydney, New South Wales, Australia. [11]These authors contributed equally: Benedikt Brommer, Xiao Tian, Anitha Krishnan, Margarita Meer. [12]These authors jointly supervised this work: Meredith S. Gregory-Ksander, Bruce R. Ksander, Zhigang He, David A. Sinclair. ✉e-mail: david_sinclair@hms.harvard.edu

is an oncogene that reduces the lifespan of mice[20] and is not required for the initiation of cellular reprogramming[21]. We therefore excluded MYC from our experiments and expressed only the transcription factors OCT4, SOX2 and KLF4 (OSK) in fibroblasts from old mice, after which we monitored the effect on genes that are known to be altered with age, including *Lmnb1*, *Chaf1b*, and those from the H2a and H2b families[13]. Even without MYC, the expression of OSK for five days promoted a youthful mRNA profile, with no apparent loss of cellular identity or induction of NANOG—a transcription factor that is indicative of pluripotency and oncogenicity (Extended Data Fig. 1a–c).

Next we tested the long-term safety of ectopically expressing OSK in vivo. To deliver and control OSK expression in mice, we engineered a dual adeno-associated virus (AAV) system under the tight control of a tetracycline response element (TRE) promoter (Fig. 1a). The TRE promoter can be activated either by reverse tetracycline-controlled transactivator (rtTA) in the presence of the tetracycline derivative doxycycline (DOX) ('Tet-On') or by tetracycline-controlled transactivator (tTA) in the absence of DOX ('Tet-Off'). Extraneous AAV sequences were removed from the vector to accommodate OSK as a polycistron. To test if AAV-mediated OSK expression was toxic in vivo, we co-infected young (5-month-old) and aged (20-month-old) mice with AAV9-rtTA;TRE-OSK via intravenous delivery. OSK expression was then induced by providing DOX in the drinking water, our rationale being that the weak tropism of AAV for the digestive system might avoid the dysplasia and weight loss that is seen in transgenic mouse models[18] (Extended Data Fig. 1d–i). After 10–18 months of continuous OSK induction, no increase in tumour incidence or negative effects on overall health were observed, indicating that cellular identity was maintained in OSK-expressing cells (Extended Data Fig. 1j–n).

## OSK stimulates axon regeneration

Almost all species experience a decline in regenerative potential during ageing. In mammals, one of the first systems to lose regenerative potential is the CNS[5–7]. Retinal ganglion cells (RGCs) of the CNS project axons away from the retina to form the optic nerve. If damaged, RGCs of embryos and neonates can regenerate axons, but this capacity is lost within days after birth, probably due to a molecular program that is intrinsic to the RGCs[6,22]. Attempts to reverse optic-nerve damage have been only moderately successful, and there are currently no treatments that can restore eyesight either in late-stage glaucoma or in old age[23].

To test whether it is possible to provide adult RGCs with the regenerative capacity of younger RGCs, we induced OSK in an optic-nerve crush-injury model. To deliver genes into the retina, Tet-Off AAV2s carrying an OSK polycistron were injected into the vitreous body, resulting in DOX-responsive OSK gene expression in around 40% of RGCs, as estimated by immunostaining (Fig. 1b, Extended Data Fig. 2a, b). Even after 15 months of continuous induction, OSK expression did not induce any tumours or structural changes in the retina (Extended Data Fig. 2c–i, Supplementary Videos 1–3).

In a separate cohort, RGCs were infected with Tet-Off AAV2 and optic-nerve crush was performed two weeks later (Fig. 1c). After another two weeks, Alexa Fluor 555-conjugated cholera toxin subunit B (CTB)—an anterograde axonal tracer—was delivered by intravitreal injection to quantify axon regeneration. Independent of RGC proliferation (Extended Data Fig. 3a, b), the greatest extent of axon regeneration and RGC survival occurred when all three genes were delivered and expressed as a polycistron within the same AAV particle (Fig. 1d, e). Notably, when polycistronic OSK was induced for 12–16 weeks, regenerating and sprouting RGC axon fibres extended over 5 mm into the chiasm, where the optic nerve connects to the brain (Extended Data Fig. 3c, d). Suppression of polycistronic OSK by DOX treatment prevented both regenerative and survival effects (Fig. 1d, e, Extended Data Fig. 3e).

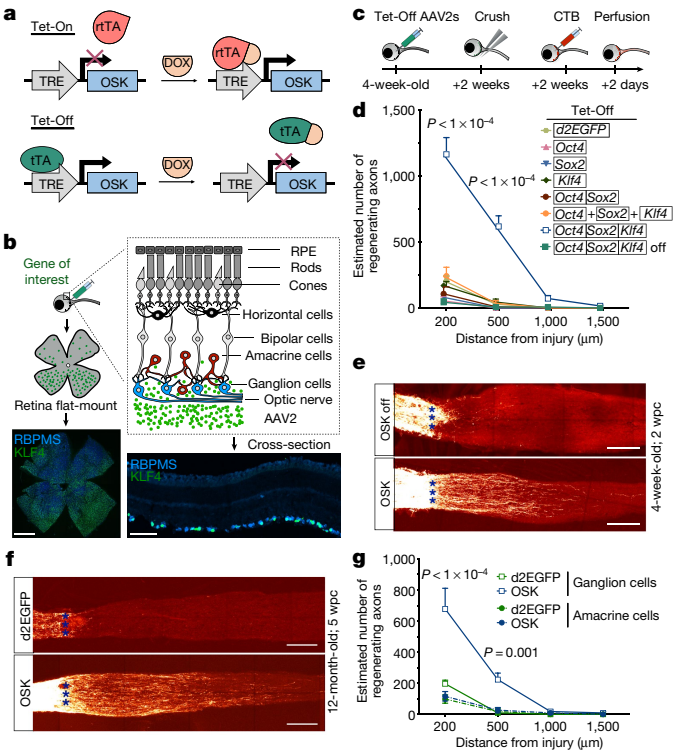


**Fig. 1 | AAV2-delivered polycistronic OSK promotes axon regeneration and RGC survival after optic nerve injury. a**, Schematic of the Tet-On and Tet-Off dual AAV vectors. OSK denotes *Oct4*-P2A-*Sox2*-T2A-*Klf4*. **b**, Schematic (top) and representative retinal wholemount (bottom left) and cross-sections (bottom right) ($n = 10$), two weeks after intravitreal injection of AAV2-tTA;TRE-OSK, showing *Klf4* (green) expression in the RGCs (blue, visualized by RBPMS as marker). Scale bars, 1 mm (left); 100 μm (right). **c**, Experimental outline of the optic-nerve crush-injury study using the Tet-Off system. 555-CTB was used for anterograde axonal tracing. **d**, The number of axons 16 days after crush injury, at distances distal to the lesion, in mice treated with AAV2 encoding: destabilized enhanced green fluorescent protein (d2EGFP); *Oct4*; *Sox2*; *Klf4*; *Oct4* and *Sox2*; all three OSK genes on three monocistronic AAV2s (indicated as separated by + signs); or all three OSK genes on a single polycistronic AAV2 ($n = 5, 4, 4, 4, 4, 4$ and 7 eyes, respectively). In **d**, **e**, suppression of polycistronic OSK expression by DOX ($n = 5$ eyes) is shown as OSK off. **e**, Representative images of longitudinal sections through the optic nerves of 4-week-old (young) mice after receiving intravitreal injections of AAV2-tTA;TRE-OSK in the presence ($n = 5$) or absence ($n = 7$) of DOX. CTB-labelled axons are shown 16 days post-crush. Asterisks indicate the optic-nerve crush site. **f**, Representative confocal images of longitudinal sections through the optic nerve showing CTB-labelled axons in 12-month-old (old) mice, 5 weeks post-crush, with AAV2-mediated expression of either GFP or OSK. Representative results from $n = 5$ eyes. Scale bars (**e**, **f**), 200 μm. **g**, The number of axons 16 days post-crush at multiple distances distal to the lesion site in transgenic Cre lines that selectively express OSK either in RGCs (Vglut2-Cre) or in amacrine cells (Vgat-Cre) after intravitreal injection of AAV2-FLEx-tTA;TRE-OSK ($n = 4$ eyes for each condition). Further details are given in Extended Data Fig. 4e–h. One-way ANOVA with Bonferroni correction (**d**, **g**), with comparisons to d2EGFP shown in **f**. All data are presented as mean ± s.e.m.

When *Oct4*, *Sox2* and *Klf4* were co-delivered by separate monocistronic AAVs, no effect on axon regeneration was observed; this was ostensibly due to the lower frequency of co-infection or inconsistent stoichiometry (Fig. 1d, Extended Data Fig. 3f–i). When delivered singly, *Oct4* or *Sox2* alone increased RGC survival slightly (Extended Data Fig. 3e), but none of the single factors alone had any effect on regenerative capacity (Fig. 1d). Because *Klf4* can repress rather than promote axonal growth[24], we tested a dual-cistron of only *Oct4* and *Sox2* and observed no regenerative effect.

Many regenerative approaches that work well in young individuals often fail in older ones[25,26]. In 12-month-old mice, OSK treatment doubled RGC survival, similar to the results observed in 1- and 3-month-old mice (Extended Data Fig. 4a). Although axon regeneration was slightly weaker in the older mice (Extended Data Fig. 4b), when treatment was extended for 3 more weeks (thus measuring regeneration 5 weeks after the optic-nerve crush), robust axon regeneration still occurred, with no increase in RGC number (Fig. 1f, Extended Data Fig. 4c, d). These data indicate that ageing does not greatly diminish the ability of OSK transcription factors to induce axon regeneration.

To test whether OSK was acting directly on RGCs or through amacrine cells[27]—the other type of retinal cells that AAV2 can infect after intravitreal injection—we introduced tTA in a double-floxed inverse orientation (AAV2-FLEx-tTA) with AAV2-TRE-OSK into two Cre transgenic mouse lines, so that OSK was selectively expressed either in RGCs (Vglut2-Cre) or amacrine cells (Vgat-Cre) (Extended Data Fig. 4e, f). OSK expression in RGCs alone promoted axon regeneration, whereas expression in amacrine cells did not (Fig. 1g, Extended Data Fig. 4g, h). The survival frequency of OSK-positive RGCs was roughly three times that of nearby OSK-negative cells or that of RGCs in GFP-expressing retinas, resulting in a greater relative abundance of OSK-positive RGCs after injury (Extended Data Fig. 4i–k). Therefore, the ability of OSK to increase survival seems to be mediated within the RGC and is largely cell-autonomous. The mRNA levels of *Stat3*, a pro-regeneration gene[28], robustly increased in response to OSK and were maintained post-injury (Extended Data Fig. 5a, Supplementary Table 1). *Stat3* upregulation, however, does not seem to be mediated by the PTEN–mTOR–S6K or the SOCS3 pathways, two canonical *Stat3* regulatory pathways that affect RGC axon regeneration[29,30] (Extended Data Fig. 5b, c, Supplementary Table 1).

## OSK counters injury-induced DNA methylation ageing

Currently, there is no known treatment that can induce robust RGC axon regeneration when the treatment is started after crush injury. Using our Tet-On AAV system, which rapidly induces OSK expression (Fig. 2a, Extended Data Figs. 2b, 5d, e), we observed significant improvement in axon regeneration and RGC survival, even when OSK was induced after injury. The longer the duration of the OSK induction the greater the distance the axons extended, with no sign of RGC proliferation (Fig. 2b, c, Extended Data Fig. 5f).

Given the effectiveness of OSK induction after injury and the ability of Yamanaka factors to reverse DNA methylation age in vitro[4,15,31,32], we speculated that OSK might act to regenerate axons by counteracting the effect of injury on DNA methylation. The DNA methylation age of RGCs was calculated on the basis of a ribosomal DNA methylation clock[33], which provided the best site coverage (67 out of 72 CpG sites) and was highly correlated with chronological age (Extended Data Fig. 5g). At day 4 after injury, RGCs experienced an acceleration of DNA methylation age, whereas OSK expression counteracted this effect (Fig. 2d). Patterns of global DNA methylation were also altered by injury in a manner similar to that of ageing, without affecting average DNA methylation levels (Extended Data Fig. 5h, i). Notably, OSK reversed the global DNA methylation changes caused by injury, and this reversal was enriched at genes that are associated with light detection and synaptic transmission (Fig. 2e, Extended Data Fig. 5j, k).

## Regeneration requires DNA demethylation

Next we asked whether the DNA methylation changes induced by OSK are necessary for RGC survival and axon regrowth. DNA demethylation is catalysed by ten-eleven translocation methylcytosine dioxygenases (TET1–TET3), either passively through DNA replication or actively—even in non-replicating cells—by reversion to cytosine via thymine DNA glycosylase (TDG)[34]. Because TET1 and TET2—but not TET3—were

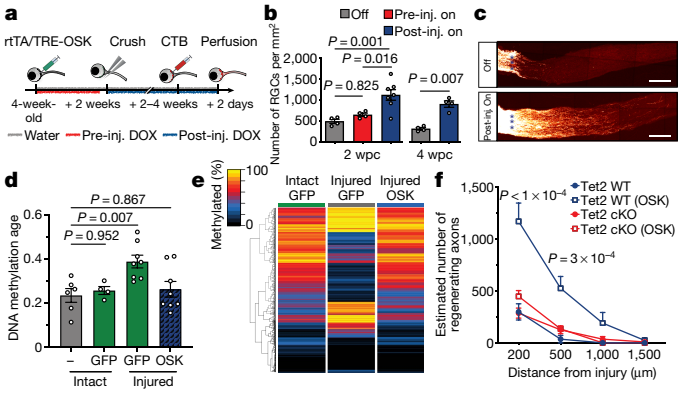


**Fig. 2 | DNA demethylation is required for OSK-induced axon regeneration after injury. a**, Strategies for induction of OSK pre- and post-injury. **b**, Survival of RGCs (number of RGCs per mm$^2$) at 2 and 4 weeks post-crush (wpc) in response to OSK induction either pre- or post-injury (inj.) ($n = 4$ eyes, except for the post-injury 'on' group at 2 weeks post-crush, for which $n = 7$ eyes). **c**, Representative longitudinal sections through the optic nerve showing CTB-labelled axons at 4 weeks post-crush, without (top) or with (bottom) the induction of OSK after injury. Asterisks indicate the optic-nerve crush site. Results are representative from $n = 4$ eyes. Scale bars, 200 μm. **d**, Ribosomal DNA methylation age (in months) of 6-week-old RGCs isolated from axon-intact retinas infected with or without GFP-expressing AAV2 (intact), or from axon-injured retinas infected with GFP- or OSK-expressing AAV2 at 4 days post-crush (injured) ($n = 6$, 4, 8 and 8 eyes, respectively). DNA methylation age estimates of neurons tend to be lower than their chronological ages but remain correlated (see Extended Data Fig. 5g and Methods). **e**, Hierarchical clustered heat map of DNA methylation levels of CpGs that significantly changed in RGCs after crush injury (intact GFP vs injured GFP, $q < 0.05$) and the effect of OSK at 4 days post-crush (injured OSK). **f**, Axon regeneration in response to OSK expression (AAV2-tTA; TRE-OSK), 16 days post-crush in *Tet2*$^{flox/flox}$ mice infected with saline (Tet2 wild type (WT); $n = 3$ for each condition) or AAV2-Cre (Tet2 cKO; $n = 4$ for each condition). One-way ANOVA with Bonferroni's multiple comparison test (**b**, **d**, **f**). For all bar graphs, data are mean ± s.e.m.

upregulated by OSK[35,36] (Extended Data Fig. 6a), we tested the effect of knocking down their encoding genes *Tet1* or *Tet2* (using short hairpin (sh)RNA delivered by AAV[37]) in the context of damaged, OSK-treated RGCs (Extended Data Fig. 6b–d).

The knockdown of either *Tet1* or *Tet2* blocked the ability of OSK to increase *Stat3* mRNA levels and to promote RGC survival and axon regeneration (Extended Data Fig. 6e–g). Knocking out *Tet2* in RGCs by delivering AAV2-Cre[30] intravitreally to *Tet2*$^{flox/flox}$ mice also abrogated the increase in regeneration and survival (Fig. 2f, Extended Data Fig. 6h–j). OSK-expressing RGCs showed no evidence of DNA replication in a 5-bromo-2′-deoxyuridine (BrdU) assay (Extended Data Fig. 3a, b), and knockdown of *Tdg*[38] completely abolished the beneficial effects of OSK (Extended Data Fig. 7a–d); however, a global reduction of DNA methylation mediated by overexpression of the TET1 catalytic domain[39] had no protective or regenerative effect (Extended Data Fig. 7e–h). These data indicate that active DNA demethylation is necessary—but is not sufficient by itself—in order for OSK to protect RGCs and to regenerate axons (Extended Data Fig. 7i).

## Axon regeneration in human neurons

Paralleling the mouse RGC data, the expression of OSK in differentiated human neurons effectively counteracted axonal loss and the advancement of DNA methylation age induced by vincristine—a chemotherapeutic drug that induces axon injury—in the absence of cell proliferation or global DNA demethylation (Extended Data Fig. 8a–g). Nine days after damage, the neurite area was 15-fold greater in the rejuvenated OSK-transduced cells compared with control cells (Extended Data Fig. 8h, i).

OSK-mediated recovery of the neurite area, as well as both the number and the length of axons, were blocked by *Tet2* knockdown but not by inhibition of the mTOR–S6K pathway (Extended Data Fig. 8j–s). Again, overexpression of the TET1 catalytic domain alone failed to promote axon regeneration (Extended Data Fig. 8t). The ability of OSK to reprogram neurons and to promote axon growth in a *Tet2*-dependent manner therefore seems to be conserved across mice and humans.

## Recovery of vision in mice with glaucoma

We then tested whether OSK induction could restore the function of RGCs in a disease setting. Glaucoma, a leading cause of age-related blindness worldwide, is characterized by a progressive loss of RGCs and their axons, and often coincides with increased intraocular pressure. We induced increased intraocular pressure unilaterally for 21 days by injecting microbeads into the anterior chamber of the eye[40] (Fig. 3a, b), using saline injections as non-glaucomatous controls. At the 4-week time point, after a significant decrease in axonal density and the number of RGCs (baseline, Extended Data Fig. 9a, b), AAVs were injected intravitreally and OSK expression was induced for another 4 weeks (Fig. 3a). Compared with glaucomatous eyes that received either PBS or AAVs with no OSK induction (−OSK), the OSK-treated glaucomatous eyes (+OSK) presented with a restored axon density equivalent to that in the non-glaucomatous eyes, with no evidence of RGC proliferation (Extended Data Fig. 9c, d).

A significant increase in visual acuity relative to the pre-treatment function baseline was observed for eyes treated with OSK: the optomotor response assay indicated that half of the visual acuity lost from increased intraocular pressure was restored (Fig. 3c, d). A similar improvement associated with OSK expression was also seen in pattern electroretinogram (PERG) analysis (N1+P1), a readout of electrical waves generated specifically by RGCs (Fig. 3e, f). To our knowledge, this is the first example of vision-loss reversal after glaucomatous injury has occurred; previous attempts have focused on neuroprotection delivered at an early stage to prevent further disease progression[41,42] (Supplementary Information).

## Restoration of vision in old mice

The finding that OSK induction could effectively restore the DNA methylation age of RGCs after injury indicated that vision loss caused by natural ageing might be reversible too. To test this, we treated 3- and 11-month-old mice with OSK AAVs and induced OSK expression for 4 weeks (Fig. 4a). Optomotor response and PERG measurements were then carried out. In the absence of OSK induction, there was a significant reduction in visual acuity and in RGC electrical activity by 12 months of age—a loss that was restored by OSK induction (Fig. 4b, Extended Data Fig. 9e). Restoration of visual acuity was not seen in 18-month-old mice (Extended Data Fig. 9e, f), probably because assessment was hindered by an age-dependent increase in corneal opacity[43].

Because there was no obvious increase in the number of RGCs or in axon density in the 12-month-old mice treated with +OSK AAV (Extended Data Fig. 9g, h), we hypothesized that the visual improvements were due to transcriptomic changes. RGCs from 12-month-old mice, either untreated or treated with AAVs for 4 weeks, were purified by fluorescence-activated cell sorting and analysed by RNA sequencing. Compared with RGCs from young (5-month-old) mice, the mRNA levels of 464 genes were altered during ageing. Around 90% of these were restored to youthful levels by OSK treatment (Fig. 4c, d, Extended Data Fig. 9i, Supplementary Table 2). Of the 268 age-downregulated genes, 44 are linked to sensory perception and axon targeting[44], raising the possibility that they contribute to the decline in vision caused by ageing (Fig. 4d, Extended Data Figs. 9j, 10a). Another 196 genes that were upregulated during ageing are involved in ion transport or neuronal projection development, including *Efemp1* (Extended Data Fig. 10b–d), a TET1- and TET2-regulated gene that is associated with glaucoma[45] and age-related macular degeneration[46].

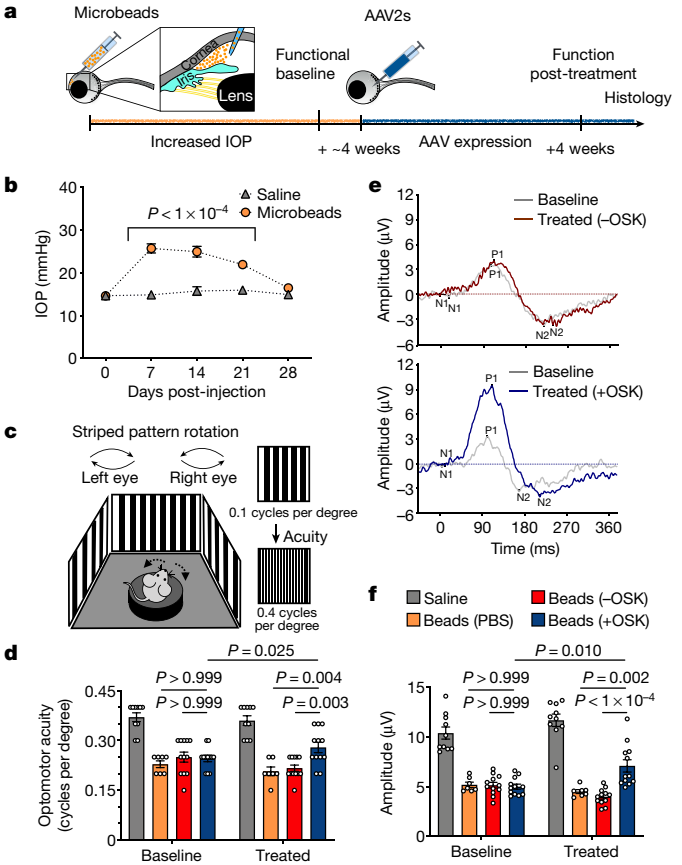


**Fig. 3 | Four weeks of OSK expression reverses vision loss after glaucomatous damage has already occurred. a**, Experimental outline of the induced glaucoma studies using 8-week-old mice. **b**, Intraocular pressure (IOP) measured weekly by rebound tonometry for the first 4 weeks after the injection of microbeads ($n = 29$ mice) or saline ($n = 10$ mice). **c**, High-contrast visual stimulation to measure optomotor response. Reflexive head movements were tracked in response to the rotation of a moving striped pattern that increased in spatial frequency. **d**, Optomotor response of each mouse before treatment (baseline) and 4 weeks after intravitreal injection of AAVs (treated; see **f** for key) ($n = 10, 7, 12$ and 12 mice for each condition; similar results from 3 independent experiments combined). **e**, Representative PERG waveforms in response to a reversing contrast checkerboard pattern, recorded from the same eye both at the pre-injection baseline and at 4 weeks after −OSK (top) or +OSK (bottom) AAV injection. **f**, Mean PERG amplitudes of recordings from each mouse in **d** at the baseline before treatment and at 4 weeks after intravitreal AAV injection ($n = 10, 7, 12$ and 12 mice for each condition; similar results from 3 independent experiments combined). −OSK (not induced), AAV2-rtTA;TRE-OSK; +OSK (induced), AAV2-tTA;TRE-OSK. For **b**, a two-way ANOVA with Bonferroni correction between groups was used; for **d**, **f**, a two-way mixed ANOVA with Bonferroni correction between groups was used for the overall effect of time and treatment, and before and after treatments were analysed using a paired two-tailed Student's *t*-test. Data in **b**, **d** and **f** are presented as mean ± s.e.m.

To gain insights into how DNA methylation changes might be involved in the effects of OSK, we used machine learning to identify a methylation ageing signature based on 1,226 sites from genome-wide DNA methylation datasets, derived from the first principal component (PC1) in multi-age training samples (Extended Data Fig. 10e, Supplementary Table 3). In an independent set of test samples, OSK reversed the DNA methylation ageing signature in the context of both injury and ageing (Fig. 4e, Extended Data Fig. 10f). Notably, the signature CpG sites were associated with genes that are involved in synaptic and neuronal processes and are enriched for the binding of polycomb repressive complex

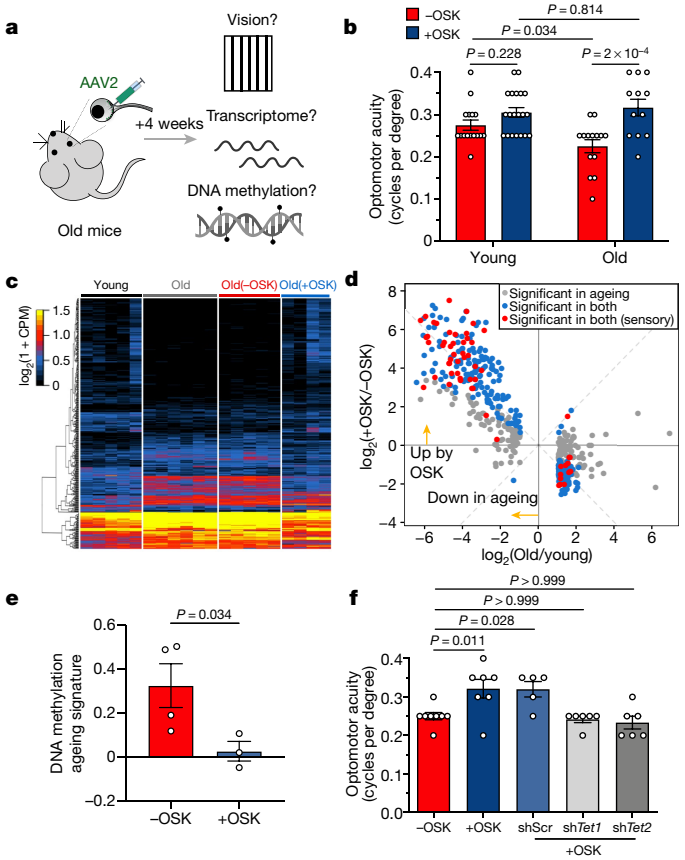


**Fig. 4 | Restoration of youthful vision, transcriptome and DNA methylation ageing signature in old mice. a**, Experimental outline for testing the effect of reprogramming in old mice. **b**, Visual acuity in young (4-month-old) and old (12-month-old) mice after 4 weeks of −OSK or +OSK treatment ($n = 16, 20, 14$ and 12 eyes, respectively; similar results from 2 independent experiments combined). **c**, **d**, Hierarchical clustered heat map (**c**) and scatter plot (**d**) showing mRNA levels of 464 genes that were differentially expressed between young and old RGCs and the effect of OSK. RGCs were sorted from the retinas of untreated young (5-month-old, $n = 5$), old (12-month-old, $n = 6$) or treated old (12-month-old; −OSK, $n = 5$; +OSK, $n = 4$) mice. The gene selection criteria for **c**, **d** are described in Methods. **e**, DNA methylation ageing signatures of RGCs from 12-month-old mice infected for 4 weeks with −OSK or +OSK ($n = 4$ and 3 retinas). **f**, Visual acuity in old (12-month-old) mice treated for 4 weeks with −OSK, +OSK, or +OSK together with short hairpin scramble RNA (shScr), shTet1 or shTet2 ($n = 8, 7, 5, 6$ and 6 eyes, respectively). −OSK: AAV2-rtTA;TRE-OSK (**b**); AAV2-TRE-OSK (**c**, **d**); AAV2-tTA;TRE-d2EGFP (**e**); +OSK: AAV2-tTA;TRE-OSK (**b**–**f**). Two-way ANOVA with Bonferroni correction (**b**); Kruskal–Wallis test (**e**); one-way ANOVA with Bonferroni correction, with comparisons to the −OSK group (**f**). For all bar graphs, data are mean ± s.e.m.

2 (PRC2) and its histone methyltransferase product—trimethylated Lys27 of histone H3 (H3K27me3)—both of which are known to recruit TET enzymes[47,48] (Extended Data Fig. 10g–i). Knockdown of either *Tet1* or *Tet2* altered the methylation status of the signature CpG sites in a similar manner and counteracted the effect of OSK on DNA methylation age (Extended Data Fig. 10j–l). Both *Tet1* and *Tet2* were also required for the improvement of RGC function and vision in 12-month-old mice (Fig. 4f, Extended Data Fig. 10m), indicating that changes in DNA methylation might have a functional role in the restoration of vision in old mice by OSK.

## Discussion

Here we show that it is possible to safely reverse the age of a complex tissue and restore its biological function in vivo. Using the eye as a model system, we present evidence that the ectopic expression of OSK transcription factors safely induces in vivo epigenetic restoration of aged CNS neurons, without causing a loss of cell identity or pluripotency. Instead, OSK promotes a youthful epigenetic signature and gene-expression pattern that causes the neurons to function as though they were young again. The requirement for active demethylation in this process supports the idea that changes in DNA methylation patterns are involved in the ageing process and its functional reversal (Extended Data Fig. 10n). However, we do not wish to imply that DNA methylation is the only epigenetic mark involved in this process. It is likely to involve other transcription factors and epigenetic modifications, such as the PRC2 complex and H3K27me3, both of which are involved in maintaining stem cell plasticity and are associated with DNA methylation clock sites[4,49,50].

Perhaps the most interesting question raised by these data is how cells encode and store youthful epigenetic information. Possibilities for information storage include covalent DNA modifications, DNA-binding proteins, RNA-guided chromatin modifying factors, and RNA–DNA hybrids that are established early in life. The role of these youth marks would be akin to the 'observer' in information theory, which preserves an original backup copy of information in case it is lost or obscured by noise[11]. We suggest that epigenetic reprogramming, either by gene therapy or other means, could promote tissue repair and the reversal of age-related decline in humans.

## Online content

Any methods, additional references, Nature Research reporting summaries, source data, extended data, supplementary information, acknowledgements, peer review information; details of author contributions and competing interests; and statements of data and code availability are available at https://doi.org/10.1038/s41586-020-2975-4.


1. Sinclair, D. A., Mills, K. & Guarente, L. Accelerated aging and nucleolar fragmentation in yeast sgs1 mutants. *Science* **277**, 1313–1316 (1997).
2. Imai, S. & Kitano, H. Heterochromatin islands and their dynamic reorganization: a hypothesis for three distinctive features of cellular aging. *Exp. Gerontol.* **33**, 555–570 (1998).
3. Oberdoerffer, P. et al. SIRT1 redistribution on chromatin promotes genomic stability but alters gene expression during aging. *Cell* **135**, 907–918 (2008).
4. Horvath, S. DNA methylation age of human tissues and cell types. *Genome Biol.* **14**, 3156 (2013).
5. Kennard, M. A. Relation of age to motor impairment in man and in subhuman primates. *Arch. Neurol. Psychiatry* **44**, 377–397 (1940).
6. Goldberg, J. L., Klassen, M. P., Hua, Y. & Barres, B. A. Amacrine-signaled loss of intrinsic axon growth ability by retinal ganglion cells. *Science* **296**, 1860–1864 (2002).
7. Yun, M. H. Changes in regenerative capacity through lifespan. *Int. J. Mol. Sci.* **16**, 25392–25432 (2015).
8. Waddington, C. H. & Kacser, H. *The Strategy of the Genes: a Discussion of Some Aspects of Theoretical Biology* (Allen & Unwin, 1957).
9. Sen, P., Shah, P. P., Nativio, R. & Berger, S. L. Epigenetic mechanisms of longevity and aging. *Cell* **166**, 822–839 (2016).
10. Sinclair, D. A. & LaPlante, M. D. *Lifespan: Why We Age—and Why We Don't Have To* 13–23, 158–175 (Simon & Schuster, 2019).
11. Shannon, C. E. A mathematical theory of communication. *Bell Syst. Tech. J.* **27**, 379–423 (1948).
12. López-Otín, C., Blasco, M. A., Partridge, L., Serrano, M. & Kroemer, G. The hallmarks of aging. *Cell* **153**, 1194–1217 (2013).
13. Yang, J.-H. et al. Erosion of the epigenetic landscape and loss of cellular identity as a cause of aging in mammals. Preprint at https://doi.org/10.1101/808642 (2019).
14. Takahashi, K. & Yamanaka, S. Induction of pluripotent stem cells from mouse embryonic and adult fibroblast cultures by defined factors. *Cell* **126**, 663–676 (2006).
15. Petkovich, D. A. et al. Using DNA methylation profiling to evaluate biological age and longevity interventions. *Cell Metab.* **25**, 954–960.e6 (2017).
16. Ocampo, A. et al. In vivo amelioration of age-associated hallmarks by partial reprogramming. *Cell* **167**, 1719–1733.e12 (2016).
17. Ohnishi, K. et al. Premature termination of reprogramming in vivo leads to cancer development through altered epigenetic regulation. *Cell* **156**, 663–677 (2014).
18. Abad, M. et al. Reprogramming in vivo produces teratomas and iPS cells with totipotency features. *Nature* **502**, 340–345 (2013).
19. Senís, E. et al. AAV vector-mediated in vivo reprogramming into pluripotency. *Nat. Commun.* **9**, 2651 (2018).
20. Hofmann, J. W. et al. Reduced expression of MYC increases longevity and enhances healthspan. *Cell* **160**, 477–488 (2015).

21. Rand, T. A. et al. MYC releases early reprogrammed human cells from proliferation pause via retinoblastoma protein inhibition. *Cell Rep*. **23**, 361–375 (2018).
22. Laha, B., Stafford, B. K. & Huberman, A. D. Regenerating optic pathways from the eye to the brain. *Science* **356**, 1031–1034 (2017).
23. Roska, B. & Sahel, J. A. Restoring vision. *Nature* **557**, 359–367 (2018).
24. Moore, D. L. et al. KLF family members regulate intrinsic axon regeneration ability. *Science* **326**, 298–301 (2009).
25. Geoffroy, C. G., Hilton, B. J., Tetzlaff, W. & Zheng, B. Evidence for an age-dependent decline in axon regeneration in the adult mammalian central nervous system. *Cell Rep*. **15**, 238–246 (2016).
26. Yao, K. et al. Restoration of vision after de novo genesis of rod photoreceptors in mammalian retinas. *Nature* **560**, 484–488 (2018).
27. Zhang, Y. et al. Elevating growth factor responsiveness and axon regeneration by modulating presynaptic inputs. *Neuron* **103**, 39–51.e5 (2019).
28. Luo, X. et al. Enhanced transcriptional activity and mitochondrial localization of STAT3 co-induce axon regrowth in the adult central nervous system. *Cell Rep*. **15**, 398–410 (2016).
29. Park, K. K. et al. Promoting axon regeneration in the adult CNS by modulation of the PTEN/mTOR pathway. *Science* **322**, 963–966 (2008).
30. Sun, F. et al. Sustained axon regeneration induced by co-deletion of PTEN and SOCS3. *Nature* **480**, 372–375 (2011).
31. Olova, N., Simpson, D. J., Marioni, R. E. & Chandra, T. Partial reprogramming induces a steady decline in epigenetic age before loss of somatic identity. *Aging Cell* **18**, e12877 (2019).
32. Sarkar, T. J. et al. Transient non-integrative expression of nuclear reprogramming factors promotes multifaceted amelioration of aging in human cells. *Nat. Commun*. **11**, 1545 (2020).
33. Wang, M. & Lemos, B. Ribosomal DNA harbors an evolutionarily conserved clock of biological aging. *Genome Res*. **29**, 325–333 (2019).
34. Wu, X. & Zhang, Y. TET-mediated active DNA demethylation: mechanism, function and beyond. *Nat. Rev. Genet*. **18**, 517–534 (2017).
35. Koh, K. P. et al. Tet1 and Tet2 regulate 5-hydroxymethylcytosine production and cell lineage specification in mouse embryonic stem cells. *Cell Stem Cell* **8**, 200–213 (2011).
36. Gao, Y. et al. Replacement of Oct4 by Tet1 during iPSC induction reveals an important role of DNA methylation and hydroxymethylation in reprogramming. *Cell Stem Cell* **12**, 453–469 (2013).
37. Yu, H. et al. Tet3 regulates synaptic transmission and homeostatic plasticity via DNA oxidation and repair. *Nat. Neurosci*. **18**, 836–843 (2015).
38. Weng, Y.-L. et al. An intrinsic epigenetic barrier for functional axon regeneration. *Neuron* **94**, 337–346.e6 (2017).
39. Guo, J. U., Su, Y., Zhong, C., Ming, G. L. & Song, H. Hydroxylation of 5-methylcytosine by TET1 promotes active DNA demethylation in the adult brain. *Cell* **145**, 423–434 (2011).
40. Krishnan, A. et al. Overexpression of soluble Fas ligand following adeno-associated virus gene therapy prevents retinal ganglion cell death in chronic and acute murine models of glaucoma. *J. Immunol*. **197**, 4626–4638 (2016).
41. Almasieh, M. & Levin, L. A. Neuroprotection in glaucoma: animal models and clinical trials. *Ann. Rev. Vis. Sci*. **3**, 1–30 (2016).
42. Levin, L. A. et al. Neuroprotection for glaucoma: requirements for clinical translation. *Exp. Eye Res*. **157**, 34–37 (2017).
43. McClellan, A. J. et al. Ocular surface disease and dacryoadenitis in aging C57BL/6 mice. *Am. J. Pathol*. **184**, 631–643 (2014).
44. Li, H. et al. Single-cell transcriptomes reveal diverse regulatory strategies for olfactory receptor expression and axon targeting. *Curr. Biol*. **30**, 1189–1198.e5 (2020).
45. Mackay, D. S., Bennett, T. M. & Shiels, A. Exome sequencing identifies a missense variant in EFEMP1 co-segregating in a family with autosomal dominant primary open-angle glaucoma. *PLoS ONE* **10**, e0132529 (2015).
46. Marmorstein, L. Y. et al. Aberrant accumulation of EFEMP1 underlies drusen formation in Malattia Leventinese and age-related macular degeneration. *Proc. Natl Acad. Sci. USA* **99**, 13067–13072 (2002).
47. Wu, X., Li, G. & Xie, R. Decoding the role of TET family dioxygenases in lineage specification. *Epigenetics Chromatin* **11**, 58 (2018).
48. Neri, F. et al. Genome-wide analysis identifies a functional association of Tet1 and Polycomb repressive complex 2 in mouse embryonic stem cells. *Genome Biol*. **14**, R91 (2013).
49. Margueron, R. & Reinberg, D. The Polycomb complex PRC2 and its mark in life. *Nature* **469**, 343–349 (2011).
50. Mozhui, K. & Pandey, A. K. Conserved effect of aging on DNA methylation and association with EZH2 polycomb protein in mice and humans. *Mech. Ageing Dev*. **162**, 27–37 (2017).

# Methods

No statistical methods were used to predetermine sample size. The mice were randomly assigned to experimental groups, except in experiments that required specific genotypes. The investigators were blinded to animal allocation but not cell cultures or outcome assessment.

### Mouse lines

For optic-nerve crush and glaucoma model experiments, C57BL6/J wild type mice were purchased from the Jackson Laboratory (000664). Young and old females from the NIA Aged Rodent Colonies were used for ageing experiments. Rosa26-M2rtTA/Col1a1-tetOP-OKS-mCherry alleles were from the Hochedlinger laboratory (Massachusetts General Hospital)[51]. Rosa-CAG-lox-STOP-lox-Tomato mice were provided by F. Wang (McGovern Institute). Vglut2-IRES-Cre (016963), Vgat-IRES-Cre (016962), *Tet2*$^{flox/flox}$ (017573)[52] and Rosa26-M2rtTA/Col1a1-tetOP-OSKM (011011) were purchased from the Jackson Laboratory. All animal work was approved by the Institutional Animal Care and Use Committees (IACUCs) at Harvard Medical School, Boston Children's Hospital, and the Mass Eye and Ear Institution. Animals were housed under 12-h light/dark cycles (6:00/18:00), at an ambient temperature of 70–72 °F (21–22 °C) and 40–50% humidity.

### Surgery

Mice were anaesthetized by intraperitoneal injection of a mixture of ketamine (100 mg kg$^{-1}$; Ketaset; Fort Dodge Animal Health) and xylazine (10 mg kg$^{-1}$; TranquiVed; Vedco) supplemented by topical application of proparacaine to the ocular surface (0.5%; Bausch & Lomb). All animal procedures were approved by the IACUC of the respective institutions and according to appropriate animal welfare regulations.

### Production of adeno-associated viruses

Vectors of AAV-TRE-OSK were made by cloning mouse *Oct4*, *Sox2* and *Klf4* cDNA into an AAV plasmid consisting of the tetracycline response element (TRE3G) promoter and the SV40 element. The other home-made vectors were made using a similar strategy or directly chemically synthesized. All pAAVs, as listed (Supplementary Table 4), were then packaged into AAVs of serotype 2/2, 2/DJ or 2/9 (titres: >5 × 10$^{12}$ genome copies per ml). AAVs were produced by the Boston Children's Hospital Viral Core.

### Systemic delivery of AAV9

Expression in internal organs was achieved through retro-orbital injection of AAV9: 7 × 10$^{11}$ gene copies (gc) of UBC-rtTA and 3 × 10$^{11}$ gc of TRE-OSK for 5-month-old mice; 7 × 10$^{11}$ gc of UBC-rtTA and 5 × 10$^{11}$ gc of TRE-OSK (or TRE-GFP) for 20-month-old mice. To induce OSK expression, DOX (1 mg ml$^{-1}$; MP Biochemicals) was given in drinking water continuously until the end of the experiment, 3 weeks after AAV injection.

### Cell culture of ear fibroblasts

Ear fibroblasts were isolated from Reprogramming 4F (Jackson Laboratory 011011) or 3F (Hochedlinger laboratory, Massachusetts General Hospital) mice and cultured at 37 °C in DMEM (Invitrogen) containing non-essential amino acids, 10% tetracycline-free fetal bovine serum (TaKaRa Bio, 631106) and 1% penicillin/streptomycin (ThermoFisher Scientific, 15140122). Ear fibroblasts of transgenic mice were passaged to P3 and treated with DOX (2 μg ml$^{-1}$) for the indicated time periods in the culture medium. All cell lines used were mycoplasma negative.

### AAV2 intravitreal injection

Adult animals were anaesthetized with ketamine/xylazine (100/10 mg kg$^{-1}$), and then AAV (1–2 μl) was injected intravitreally, just posterior to the limbus with a fine glass pipette attached to a Hamilton syringe using plastic tubing. In the increased IOP model, mice received a 1 μl intravitreal injection between 3 and 4 weeks after microbead injection. The injected volume of AAV-shRNA is one-fifth the volume of other AAVs.

### Optical coherence tomography

Optical coherence tomography (OCT) images were taken with a Bioptigen Envisu R-Class OCT (Leica Microsystems). The animals were anaesthetized with a ketamine/xylazine (100-200/20 mg kg$^{-1}$) cocktail and eyes were treated with a drop of 1% tropicamide solution to dilate the pupils and a drop of GenTeal gel to keep the lens hydrated. Full retinal OCT scans were obtained for all eyes (1,000×, 100×, 10). One-hundred B-scans were converted into videos (7 frames per second (fps)) with ImageJ. Representative OCT images of the retina were taken near the head of the optic nerve, and the imaging location was marked on the volume intensity projection image with a white line. The retinal thickness in each eye was measured using 4 B-scans at a distance of 50–600 μm on both sides of the optic nerve head and averaged using ImageJ.

### Creation of retinoblastoma tumours

To create the space to inject the retinoblastoma tumour cells into the subretinal space, a transient retinal detachment was created. Intraocular pressure was decreased by first making a corneal incision, followed by a subretinal injection of 10,000 retinoblastoma tumour cells (Rb116) via a 30-gauge needle in a total volume of 10 μl. Two weeks after injection the mice were observed using OCT.

### Optic nerve crush

Two weeks after intravitreal AAV injection, the optic nerve was accessed intraorbitally and crushed in anaesthetized animals using a pair of Dumont #5 forceps (FST). Alexa-conjugated cholera toxin beta subunit (CTB-555, 1 mg ml$^{-1}$; 1–2 μl) injection was performed 2 days before euthanasia to trace regenerating RGC axons. The surgical methods have been described in more detail previously[29].

### In vivo DOX induction or suppression

Induction of the Tet-On or suppression of the Tet-Off AAV2 systems in the retina was performed by administration of DOX (2 mg ml$^{-1}$) (Sigma) in the drinking water. Induction of Tet-On AAV9 system systemically was performed by administration of DOX (1 mg ml$^{-1}$) (USP grade, MP Biomedicals 0219895505) in the drinking water.

### Quantification of axon regeneration for the optic-nerve crush model

The number of regenerating axons in the optic nerve was estimated by counting the number of CTB-labelled axons at different distances from the crush site, as described previously[29].

### Wholemount optic nerve preparation

Optic nerves and the connecting chiasm were dehydrated in methanol for 5 min, then incubated overnight with Visikol HISTO-1. The next day, nerves were transferred to Visikol HISTO-2 and then incubated for 3 h. Finally, optic nerves and connecting chiasm were mounted with Visikol HISTO-2.

### Immunofluorescence

Wholemount retinas were blocked with horse serum at 4 °C overnight then incubated at 4 °C for 3 days with primary antibodies diluted in PBS, BSA (3%) Triton X-100 (0.5%). Then, tissues were incubated at 4 °C overnight with appropriate Alexa Fluor-conjugated secondary antibodies (Alexa 405, 488, 567, 674; Invitrogen) diluted with the same blocking solution as the primary antibodies, generally used at 1:400 final dilution. Frozen sections were stained overnight with primary antibodies at 4 °C and then secondary antibodies at room temperature for 2 h. Between changes of solutions, all wholemounts or slices were washed 3 times, for 5 min each time. Sections or wholemount

retinas were mounted with Vectashield Antifade Mounting Medium. Antibodies used were as follows: mouse anti-OCT4 (1:100, BD Bioscience 611203), rabbit anti-SOX2 (1:100, Cell Signaling 14962), goat anti-KLF4 (1:100, R&D systems AF3158), tabbit anti-phosphorylated S6 Ser235/236 (1:100, Cell Signaling 4857), mouse anti-BRN3A (1:200, EMD Millipore MAB1585), rabbit anti-Ki67(1:100, Abcam ab15580), mouse anti-AP2 alpha (1:100, Developmental Studies Hybridoma Bank 3B5), rabbit anti-pSTAT3 (Tyr705) (1:100, Cell Signaling 9145S), rat anti-HA (1:400, Roche 11867423001), rabbit anti-5mC (1:100, Cell Signaling 28692S), rabbit anti-5hmC (1:100, Active Motif 39769), rat anti-BrdU (1:200, Abcam ab6326), rabbit anti-Olig2 (1:100, Novusbio NBP1-28667), chicken anti-GFP (1:10,000, Aves Labs GFP-1020) and guinea pig anti-RBPMS (1:400, Raygene custom order A008712 to peptide GGKAEKENTPSEANLQEEEVRC). Note that successful staining for anti-5mC, anti-5hmC, anti-Ki67 and anti-BrdU requires pre-treatment with 2 M HCl for 30 min at room temperature, followed by 3 washes with 0.1 M sodium borate (pH 8.3) and PBST each before the serum blocking.

### Bromodeoxyuridine labelling

After crush injury, mice were injected intraperitoneally with 5-bromo-2′-deoxyuridine (BrdU) (Sigma, B5002) at a dose of 100 mg $kg^{-1}$ daily the week before they were euthanized. Optic nerves and retinas were collected either 1 or 2 wpc. Optic nerve sections and retina wholemounts were then performed with the same procedure described for immunofluorescence (including HCl pre-treatment) to complete the staining.

### Western blot

SDS–PAGE and western blot analysis was performed according to standard procedures and detected with an ECL detection kit. Antibodies used: rabbit anti-SOX2 (1:100, EMD Millipore, AB5603), mouse anti-KLF4 (1:1,000, ReproCell, 09-0021), rabbit anti-p-S6 (S240/244) (1:1,000, CST, 2215), mouse anti-S6 (1:1,000, CST, 2317), mouse anti-β-tubulin (1:1,000, Sigma-Aldrich, 05-661), mouse anti-β-actin–Peroxidase antibody (1:20,000, Sigma-Aldrich, A3854).

### RGC survival and phospho-S6 signal

RBPMS-positive cells in the ganglion layer were stained with an anti-RBPMS antibody (1:400, Raygene custom order A008712 to peptide GGKAEKENTPSEANLQEEEVRC), and a total of four 10× fields per retina, one in each quadrant, were enumerated. The average number of viable RGCs per field was determined. Phospho-S6 (1:100, Cell Signaling 4857) staining was performed under the same conditions and the percentages of phopsho-S6-positive RGCs were obtained by comparing the value to the number of all viable RGCs in the same field.

### Human neuron differentiation and regeneration assay

We chose to use differentiated human neurons that would maintain ageing signatures[53]. SH-SY5Y neuroblastoma cells were obtained from the American Type Culture Collection (ATCC, CRL-2266). Cells were confirmed as negative for mycoplasma, then cultured in a 1:1 mixture of EMEM (ATCC, 30-2003) and F12 medium (Thermo Fisher Scientific, 11765054) supplemented with 10% FBS (Sigma, F0926) and 1% penicillin/streptomycin (Thermo Fisher Scientific, 15140122). Cells were cultured at 37 °C with 5% $CO_2$ and 3% $O_2$. Cells were passaged at around 80% confluency. SH-SY5Y cells were differentiated into neurons as previously described[54] with modifications. In brief, 1 day after plating, cell differentiation was induced for 3 days using EMEM/F12 medium (1:1) containing 2.5% FBS, 1× penicillin/streptomycin, and 10 μM all-*trans* retinoic acid (ATRA, StemCell Technologies, 72264) (Differentiation Medium 1), followed by a 3 day incubation in EMEM/F12 (1:1) containing 1% FBS, 1× penicillin/streptomycin, and 10 μM ATRA (Differentiation Medium 2). Cells were then split into 35-mm cell culture plates coated with poly-D-lysine (Thermo Fisher Scientific, A3890401). A day after splitting, neurons were matured in serum-free neurobasal/B27 plus culture medium (Thermo Fisher Scientific, A3653401) containing 1× Glutamax (Thermo Fisher Scientific, 35050061), 1× penicillin/streptomycin, and 50 ng $ml^{-1}$ BDNF (Alomone Labs) (Differentiation Medium 3) for at least 5 days. Differentiated SH-SY5Y cells were transduced with AAV.DJ vectors at $10^6$ genome copies per cell. Five days after transduction, vincristine (100 nM; Sigma, V8879) was added for 24 h to induce neurite degeneration. Neurons were then washed once with PBS and fresh Differentiation Medium 3 was added back to the plates. Neurite outgrowth was monitored for 2–3 weeks by taking phase-contrast images at 100× magnification every 3–4 days. Neurite area, axon number and length of each cluster of neurons were quantified using Image J.

### Cell cycle analysis

Cells were collected and fixed with 70% cold ethanol for 16 h at 4 °C. After fixation, cells were washed twice with PBS and incubated with PBS containing 50 μg $ml^{-1}$ propidium iodide (PI) (Biotium, 40017) and 100 μg $ml^{-1}$ RNase A (Omega) for 1 h at room temperature. PI-stained samples were analysed on a BD LSR II analyser and only single cells were gated for analysis. Cell cycle profiles were analysed using FCS Express 6 (De Novo Software).

### Human neuron DNA methylation analyses

DNA was extracted using the Zymo Quick DNA mini-prep plus kit (D4069) and DNA methylation levels were measured on Illumina 850 EPIC arrays. The Illumina BeadChip (EPIC) measured bisulfite-conversion-based, single-CpG resolution DNA methylation levels at different CpG sites in the human genome. Data were generated via the standard protocol of Illumina methylation assays (GSE147436), which quantifies methylation levels by the $\beta$ value using the ratio of intensities between methylated and unmethylated alleles. Specifically, the $\beta$ value was calculated from the intensity of the methylated ($M$ corresponding to signal A) and unmethylated ($U$ corresponding to signal B) alleles, as the ratio of fluorescent signals $\beta = \mathrm{Max}(M,0)/(\mathrm{Max}(M,0) + \mathrm{Max}(U,0) + 100)$. Thus, $\beta$ values ranged from 0 (completely unmethylated) to 1 (completely methylated). 'Noob' normalization was implemented using the 'minfi' R package[55,56]. The mathematical algorithm and available software underlying the skin and blood clock for in vitro studies (based on 391 CpGs) has been previously published[57].

### Microbead-induced increased intraocular pressure (IOP)

Increase of IOP was induced unilaterally by injection of polystyrene microbeads (FluoSpheres, Invitrogen; 15-μm diameter) to the anterior chamber of the right eye of each mouse under a surgical microscope, as previously reported[40]. In brief, microbeads were prepared at a concentration of $5.0 \times 10^6$ beads per ml in sterile physiologic saline. A 2-μl volume was injected into the anterior chamber through a trans-corneal incision using a sharp glass micropipette connected to a Hamilton syringe (World Precision Instruments) followed by an air bubble to prevent leakage. Any mice that developed signs of inflammation (clouding or an oedematous cornea) were excluded.

### IOP measurements

IOPs were measured with a rebound TonoLab tonometer (Colonial Medical Supply) as previously described[40]. Mice were anaesthetized by 3% isoflurane in 100% oxygen (induction) followed by 1.5% isoflurane in 100% oxygen (maintenance) delivered with a precision vaporizer. IOP measurement was initiated within 2–3 min after the loss of a toe or tail pinch reflex. Anaesthetized mice were placed on a platform, and the tip of the pressure sensor was placed approximately 1/8 of an inch from the central cornea. Average IOP was displayed automatically after 6 measurements after elimination of the highest and lowest values. The machine-generated mean was considered as one reading, and six readings were obtained for each eye. All IOPs were taken at the same time of day (between 10:00 and 12:00) owing to the variation of IOP throughout the day.

### Optomotor response

The visual acuity of mice was measured using an optomotor reflex-based spatial frequency threshold test[58]. Mice were able to freely move and were placed on a pedestal located in the centre of an area formed by four computer monitors arranged in a quadrangle. The monitors displayed a moving vertical black and white sinusoidal grating pattern. A blinded observer, unable to see the direction of the moving bars, monitored the tracking behaviour of the mouse. Tracking was considered positive when there was a movement of the head (motor response) to the direction of the bars or rotation of the body in the direction concordant with the stimulus. Each eye was tested separately depending on the direction of rotation of the grating. The staircase method was used to determine the spatial frequency start from 0.15 to 0.40 cycles per degree, with intervals of 0.05 cycles per degree. Rotation speed (12° $s^{-1}$) and contrast (100%) were kept constant. Responses were measured before and after treatment by individuals blinded to the group of the mouse and the treatment. Mice that had intravitreal bleeding or developed signs of inflammation (clouding or an oedematous cornea) during or post intravitreal injection were excluded from optomotor response and histological analyses. Exclusion criteria were pre-determined before experimentation.

### Pattern electroretinogram

Mice were anaesthetized with ketamine/xylazine (100 mg $kg^{-1}$ and 20 mg $kg^{-1}$) and the pupils dilated with one drop of 1% tropicamide ophthalmic solution. The mice were kept under dim red light throughout the procedure on a built-in warming plate (Celeris, Full-Field and Pattern Stimulation for the rodent model) to maintain their body temperature at 37 °C. A black and white reversing checkerboard pattern with a check size of 1° was displayed on light guide electrode-stimulators placed directly on the ocular surface of both eyes and centred with the pupil. The visual stimuli were presented at 98% contrast and constant mean luminance of 50 cd $m^{-2}$, with a spatial frequency of 0.05 cycles per degree and a temporal frequency of 1 Hz. A total of 300 complete contrast reversals of PERG were repeated twice in each eye and the 600 cycles were segmented, averaged and recorded. The averaged PERGs were analysed to evaluate the peak-to-trough N1 to P1 (positive wave) amplitude.

### Quantification of optic-nerve axons in the glaucoma model

For quantification of axons, optic nerves were dissected and fixed overnight in Karnovsky's reagent (50% in phosphate buffer). Semi-thin cross-sections of the nerve were taken at 1.0 mm posterior to the globe and stained with 1% *p*-phenylenediamine (PPD) for evaluation by light microscopy. Optic-nerve cross-sections were imaged at 60× magnification using a Nikon microscope (Eclipse E800, Nikon) with DP Controller v.1.2.1.108 and DP Manager v.1.2.1.107 software (Olympus). Six to eight non-overlapping photomicrographs were taken to cover the entire area of each optic nerve cross-section. Using ImageJ (v.2.0.0-rc-65/1.51u), a 100 µm × 100 µm square was placed on each 60× image and all axons within the square (0.01 $mm^2$) were counted using the 'threshold' and 'analyze particles' functions in ImageJ as previously described[40,58,59]. Damaged axons stain darkly with PPD and were not counted. The average axon counts in the 6–8 images were used to calculate the axon density per $mm^2$ of optic nerve. Individuals performing axon counts were blinded to the experimental groups.

### Quantification of retinal ganglion cells in the glaucoma model

For ganglion cell counting, images of wholemount retinas were acquired using a 63× oil immersion objective of the Leica TCS SP5 confocal microscope (Leica Microsystems). The retinal wholemount was divided into four quadrants and two to four images (248.53 µm × 248.53 µm in size) were taken from the midperipheral and peripheral regions of each quadrant, for a total of 12 to 16 images per retina. The images were obtained as *z*-stacks (0.5 µm), and all BRN3A-positive cells in the ganglion cell layer of each image were counted using an automated counting platform as previously described[59,60]. In brief, RGCs were counted using the 'Cell Counter' plugin (http://fiji.sc/Cell_Counter) in Fiji (ImageJ Fiji, v.2.0.0-rc-69/1.52n). Each image was loaded into Fiji, and a colour counter type was chosen to mark all BRN3A-stained RGCs within each image (0.025 $mm^2$). The average number of RGCs in the 12–16 images were used to calculate the RGC density per square millimetre of retina. Two individuals blinded to the experimental groups performed all RGC counts.

### RGC enrichment

Retinas were dissected in AMES solution (oxygenated with 95% $O_2$/5% $CO_2$), digested in papain, and dissociated to single-cell suspensions with manual trituration in ovomucoid solution. Cells were spun down at 450*g* for 8 min, and resuspended in AMES + 4%BSA to a concentration of $10^5$ cells per ml. Thy1.2-PE-Cy7 antibody (1:2,000, Invitrogen 25-0902-81) was added and incubated for 15 min, followed by washing with an excess of media. Cells were spun down at 450*g* for 8 min and resuspended again in AMES + 4%BSA at a concentration of around $7 \times 10^6$ cells per ml. The live cell marker Calcein Blue (1 µl $ml^{-1}$) was added before filtering cells through 35-µm cell strainer into fluorescence activated cell sorting (FACS) tubes. More than 10,000 high Thy1.2+ and Calcein Blue+ cells were collected using a BD FACS Aria Cell Sorter with an 130-µm nozzle. Frozen cells were sent to Genewiz for RNA extraction and ultra-low input RNA sequencing, or to Zymo Research for DNA extraction and genome-wide reduced representation bisulfite sequencing (RRBS).

### RRBS library preparation

RGC DNA from mice at different ages and treatments (Supplementary Table 5) was extracted using Quick-DNA Plus Kit Microprep Kit. Starting input genomic DNA (2–10 ng) was digested with 30 units of MspI (NEB). Fragments were ligated to pre-annealed adapters containing 5′-methylcytosine instead of cytosine according to Illumina's specified guidelines. Adaptor-ligated fragments ≥50 bp in size were recovered using the DNA Clean & Concentrator-5 (cat. no.: D4003). The fragments were then bisulfite-treated using the EZ DNA Methylation-Lightning Kit (cat. no.: D5030). Preparative-scale PCR products were purified with DNA Clean & Concentrator-5 (cat. no.: D4003) for sequencing on an Illumina HiSeq using 2 × 125 bp paired end (PE).

### DNA methylation analysis of mouse RGC

Reads were filtered using Trim Galore v.0.4.1 and mapped to the mouse genome GRCm38 using Bismark v.0.15.0. Methylation counts on both positions of each CpG site were combined. Only CpG sites covered in all samples were considered for analysis (BioProject, PRJNA655981). Two outliers were excluded by low intercorrelation (<0.93) within the batch (Supplementary Table 5). This resulted in a total of 703,583 sites covered by uniquely mapped reads. Differential methylation for each CpG site was calculated using two-tailed Student's *t*-tests on every site independently, followed by the Benjamini–Hochberg procedure to adjust for false discovery rate. The delta value between groups was calculated as the difference between the means of values in two corresponding groups of samples. Gene Ontology analysis of differentially methylated sites was performed with Cistrome-GO (http://go.cistrome.org). Owing to the repetitive nature of ribosomal DNA sequence, it is not suitable for whole genome bisulfite mapping. Thus, to determine the ribosomal DNA methylation age, reads were mapped to ribosomal DNA repeat BK000964 and the coordinates were adjusted accordingly[33]. 67 out of 72 sites with at least 10 reads per site were covered for the ribosomal DNA methylation clock, compared to 102/435 sites of the whole lifespan multi-tissue clock[61], or 248/582 and 77,342/193,651 sites (ridge) of two entire lifespan multi-tissue clocks[62]. In agreement with previous studies[57,63,64], estimates of the DNA methylation age of neurons tend to be lower than their chronological age but remain correlated.

### DNA methylation ageing signature

Sorted RGC samples were split into training and test sets, with $n = 38$ samples used for candidate CpG selection and biomarker construction and $n = 23$ samples used for validation (Supplementary Table 6, Supplementary Data and code within the Supplementary Information). The training samples included those from 1-month-old controls (1 mo; $n = 6$), 6-month-old ($n = 8$), 12-month-old ($n = 2$), 18-month-old ($n = 8$), 30-month-old ($n = 6$), 1-month-old GFP-injured ($n = 4$), 12-month-old GFP ($n = 2$) and 12-month-old OSK ($n = 2$) mice. To generate a methylation ageing signature, we evaluated DNA methylation associations with three traits: age, injury and OSK treatment. To avoid batch effects, subsamples were evaluated separately as 6-month-old and 18-month-old in Batch 1, and 1-month-old, 12-month-old and 30-month-old in Batch 2 (Supplementary Table 5). Biweight midcorrelation was used to assess age trends for CpGs. Given that the second batch included samples from developing (1-month-old) mice, we applied a transformation to age that has been used in development of human epigenetic clocks when prenatal and/or developmental samples are included[4]. This transformation accounts for nonlinear changes during development. Biweight midcorrelation was then applied to test the associations of CpGs changes after injury and OSK treatment, and results were compared across the four tests. CpGs were selected if they were consistently in the top 30% of CpGs with the strongest absolute biweight midcorrelations in all four tests and showed consistency in the directionality of their associations (for example, hypomethylated with age in both batches, hypomethylated with injury, and hypermethylated after OSK). Of the 703,583 CpGs that were considered, 1,226 were selected (723 that trended towards hypermethylation with age and 503 that trended towards hypomethylation with age, see Supplementary Table 3). Principal component analysis (PCA) was conducted using the training samples from 1-month-old, 12-month-old and 30-month-old controls ($n = 14$). PC1 explained 25% of the variance in this sample. When applying an elastic net model to train a predictor of age, PCs beyond PC1 did not increase the robustness of the age prediction[65]. Thus, PC1 was used to represent the ageing signature and was standardized to have a mean = 0 and s.d. = 1. Analyses of the ageing signature in independent validation samples were then conducted to test associations with age, injury and OSK.

### Transcription-factor binding and histone modification enrichment

To identify factors that may mediate epigenetic reprogramming in RGCs, we performed transcription factor (TF) binding enrichment and histone modification enrichment analyses using the genome coordinates (GRCm38/mm10) of the 1,226 selected CpGs using the CistromeDB Toolkit (http://dbtoolkit.cistrome.org). A sensitivity analysis was conducted by performing TF and histone enrichment for five sets of 1,226 random CpGs from the 702,357 unselected sites, which was then compared against the enrichment for our selected set in order to identify TFs and histone marks that were specific to the selected set but not to CpGs in general.

### Total RNA extraction and sample quality control

Total RNA was extracted following the TRIzol Reagent User Guide (Thermo Fisher Scientific). Glycogen (1 µl of 10 mg ml$^{-1}$ solution) was added to the supernatant to increase RNA recovery. RNA was quantified using a Qubit 2.0 Fluorometer (Life Technologies), and RNA integrity was determined using TapeStation (Agilent Technologies).

### Ultra-low-input RNA library preparation and multiplexing

RNA samples were quantified using a Qubit 2.0 Fluorometer (Life Technologies), and RNA integrity was ascertained using a 2100 TapeStation (Agilent Technologies). RNA library preparations, sequencing reactions, and initial bioinformatics analysis were conducted at Genewiz. A SMART-Seq v4 Ultra Low Input Kit for Sequencing was used for full-length cDNA synthesis and amplification (Clontech), and Illumina Nextera XT library was used for sequencing library preparation. In brief, cDNA was fragmented and adaptors were added using Transposase, followed by limited-cycle PCR to enrich and add an index to the cDNA fragments. The final library was assessed by a Qubit 2.0 Fluorometer and an Agilent TapeStation.

### Paired-end sequencing

The sequencing libraries were multiplexed and clustered on two lanes of a flowcell. After clustering, the flowcell was loaded on the Illumina HiSeq instrument according to the manufacturer's instructions. Samples were sequenced using a 2 × 150 paired-end configuration. Image analysis and base calling were conducted by the HiSeq Control Software on the HiSeq instrument. Raw sequence data (.bcl files) generated from an Illumina HiSeq was converted into fastq files and de-multiplexed using the Illumina bcl2fastq v.2.17 program. One mismatch was allowed for index sequence identification.

### RNA sequencing analysis

Paired-end reads were aligned with hisat2 v.2.1.0[66] to the Ensembl GRCm38 primary assembly using splice junctions from the Ensembl release 84 annotation. Paired read counts were quantified using featureCounts v.1.6.4[67] using reads with a mapping quality (mapQ) value ≥ 20. Differentially-expressed genes for each pairwise comparison were identified with edgeR v.3.26[68], testing only genes with at least 0.1 counts per million (CPM) in at least three samples. Gene Ontology analysis of differentially expressed genes (BioProject PRJNA655981) was performed with AmiGO v.2.5.12[69–71]. The gene selection criteria for the experiments in Fig. 4c, 4d and Extended Data Fig. 9i, 9j are as follows: genes significantly changed during ageing ($q < 0.05$, absolute $\log_2$ fold-change > 1), not low expressed ($\log_2$(CPM) > −2) or altered by mock AAV infection (old vs old (−OSK), $q > 0.1$).

### Statistical analysis and figure preparation

Statistical analyses were performed with GraphPad Prism 7/8, using two-tailed Student's *t*-tests, one-way or two-way ANOVA. All of the statistical tests performed are indicated in the figure legends. The data are presented as mean ± s.e.m., except for the violin plots in Extended Data Fig. 8e, f, which show median and quartiles. Statistical analysis of changes to DNA methylations was performed with the SciPy package in Python. Figures were prepared using Keynote and Affinity Designer.

### Reporting summary

Further information on research design is available in the Nature Research Reporting Summary linked to this paper.

## Data availability

RRBS data for DNA methylation analysis and RNA sequencing data are available in the BioSample database (NCBI) and under BioProject PRJNA655981. Illumina Human Methylation EPIC array data are available in the Gene Expression Omnibus (GEO) database (NCBI) and under GSE147436. All other relevant data that support the findings of this study are available from the corresponding author upon reasonable request. Source data are provided with this paper.

## Code availability

The code for determining methylation ageing signatures is provided in the Supplementary Information.


51. Bar-Nur, O. et al. Small molecules facilitate rapid and synchronous iPSC generation. *Nat. Methods* **11**, 1170–1176 (2014).
52. Moran-Crusio, K. et al. Tet2 loss leads to increased hematopoietic stem cell self-renewal and myeloid transformation. *Cancer Cell* **20**, 11–24 (2011).

53. Mertens, J. et al. Directly reprogrammed human neurons retain aging-associated transcriptomic signatures and reveal age-related nucleocytoplasmic defects. *Cell Stem Cell* **17**, 705–718 (2015).
54. Shipley, M. M., Mangold, C. A. & Szpara, M. L. Differentiation of the SH-SY5Y human neuroblastoma cell line. *J. Vis. Exp.* **108**, e53193 (2016).
55. Triche, T. J., Jr, Weisenberger, D. J., Van Den Berg, D., Laird, P. W. & Siegmund, K. D. Low-level processing of Illumina Infinium DNA Methylation BeadArrays. *Nucleic Acids Res.* **41**, e90 (2013).
56. Fortin, J. P., Triche, T. J., Jr & Hansen, K. D. Preprocessing, normalization and integration of the Illumina HumanMethylationEPIC array with minfi. *Bioinformatics* **33**, 558–560 (2017).
57. Horvath, S. et al. Epigenetic clock for skin and blood cells applied to Hutchinson Gilford Progeria Syndrome and *ex vivo* studies. *Aging (Albany NY)* **10**, 1758–1775 (2018).
58. Sun, D., Moore, S. & Jakobs, T. C. Optic nerve astrocyte reactivity protects function in experimental glaucoma and other nerve injuries. *J. Exp. Med.* **214**, 1411-1430 (2017).
59. Krishnan, A., Kocab, A. J., Zacks, D. N., Marshak-Rothstein, A. & Gregory-Ksander, M. A small peptide antagonist of the Fas receptor inhibits neuroinflammation and prevents axon degeneration and retinal ganglion cell death in an inducible mouse model of glaucoma. *J. Neuroinflammation* **16**, 184 (2019).
60. Dordea, A. C. et al. An open-source computational tool to automatically quantify immunolabeled retinal ganglion cells. *Exp. Eye Res.* **147**, 1218–1235 (2013).
61. Meer, M. V., Podolskiy, D. I., Tyshkovskiy, A. & Gladyshev, V. N. A whole lifespan mouse multi-tissue DNA methylation clock. *eLife* **7**, e40675 (2018).
62. Thompson, M. J. et al. A multi-tissue full lifespan epigenetic clock for mice. *Aging (Albany NY)* **10**, 2832–2854 (2018).
63. Horvath, S. et al. The cerebellum ages slowly according to the epigenetic clock. *Aging (Albany NY)* **7**, 294–306 (2015).
64. Hoshino, A., Horvath, S., Sridhar, A., Chitsazan, A. & Reh, T. A. Synchrony and asynchrony between an epigenetic clock and developmental timing. *Sci. Rep.* **9**, 3770 (2019).
65. Levine, M. et al. A rat epigenetic clock recapitulates phenotypic aging and co-localizes with heterochromatin. *eLife* **9**, e59201 (2020).
66. Kim, D., Langmead, B. & Salzberg, S. L. HISAT: a fast spliced aligner with low memory requirements. *Nat. Methods* **12**, 357–360 (2015).
67. Liao, Y., Smyth, G. K. & Shi, W. featureCounts: an efficient general purpose program for assigning sequence reads to genomic features. *Bioinformatics* **30**, 923–930 (2014).
68. Robinson, M. D., McCarthy, D. J. & Smyth, G. K. edgeR: a Bioconductor package for differential expression analysis of digital gene expression data. *Bioinformatics* **26**, 139–140 (2010).
69. Carbon, S. et al. AmiGO: online access to ontology and annotation data. *Bioinformatics* **25**, 288–289 (2009).
70. Ashburner, M. et al. Gene Ontology: tool for the unification of biology. *Nat. Genet.* **25**, 25–29 (2000).
71. The Gene Ontology Consortium. The Gene Ontology Resource: 20 years and still GOing strong. *Nucleic Acids Res.* **47**, D330–D338 (2019).



**Acknowledgements** We thank A. Wagers, R. Mostoslavsky, Y. Shi, A. Das, A. Pogoutse, C. Petty, A. Coffey, B. Zhang, P. Dmitriev, K. Booher, E. Chen, J. Wang, D. Vogel, M. Thompson, A. Jacobi and S. Hou for advice and assistance; and Y. Weng, H. Song and F. Wang for reagents and mice. The work was supported by the Harvard Medical School Epigenetics Seed Grant and Development Grant; The Paul F. Glenn Foundation for Medical Research; a gift from E. Schulak; NIH awards R01AG019719 and R37AG028730 (to D.A.S.), R01EY026939 and R01EY021526 (to Z.H.), R01AG067782 and R01GM065204 (to V.N.G.) and R01AG065403 (to M.E.L. and V.N.G.). We thank Boston Children's Hospital Viral Core, which is supported by NIH5P30EY012196; and Schepens Eye Institute Core facilities, supported by NEI-P30EY003790. X.T. was supported by NIH award K99AG068303 and by NASA Postdoctoral Fellowship 80NSSC19K0439; D.L.V. was supported by NIH training grant T32AG023480; J.-H.Y. was partially supported by National Research Foundation of Korea (2012R1A6A3A03040476); B.R.K. was partially supported by the St Vincent de Paul Foundation and by NEI awards R24EY028767 and R01EY025794; and M.S.G.-K. by NEI award R21EY030276. We thank P. F. Glenn for his mentorship and support of ageing research.


**Author contributions** Y.L. and D.A.S. conceived the project. Y.L., X.T. and D.A.S. wrote the manuscript with input from all co-authors. Y.L. was involved in all experiments and analyses. M.S.B. and J.-H.Y. provided early training to Y.L. B.B., C.W., Q.Z., D.Y., S.Z. and Z.H. contributed to the optic nerve crush studies and imaging. A.K., D.Y., Q.Z., E.M.H., E.K., M.S.G.-K. and B.R.K. contributed to the glaucoma and ageing studies. M.M.K. and B.R.K. performed OCT imaging and analysis. M.M. and V.N.G. conducted ribosomal DNA methylation age analysis for mouse RGCs. M.E.L. developed the DNA methylation ageing signature. D.L.V. performed the RNA sequencing and gene association analysis. X.T. conducted human neuron experiments. S.H. conducted the human methylation clock analysis. X.T., J.-H.Y. and K.H. helped with the work on transgenic mouse fibroblasts. M.S.B., X.T., M.B.S., A.E.K. and L.A.R. helped with systemic AAV9 experiments. N.D. and G.M.C. helped with plasmid constructs and AAV9 production. K.C. helped with grant applications and project management.

**Competing interests** D.A.S. is a consultant to, inventor of patents licensed to, board member of and equity owner of Iduna Therapeutics, a Life Biosciences company developing epigenetic reprograming therapies. D.A.S. is an advisor to Zymo Research, an epigenetics tools company. Additional disclosures are at https://genetics.med.harvard.edu/sinclair/people/sinclair-other.php. Y.L., L.A.R. and S.H. are equity owners of Iduna Therapeutics, a Life Biosciences company. D.L.V. is an advisor to Liberty Biosecurity. M.S.B. is a shareholder in MetroBiotech. K.C. is an equity owner in Life Biosciences and affiliates. N.D. and G.M.C. are co-founders of Rejuvenate Bio. Disclosures for G.M.C. can be found at http://arep.med.harvard.edu/gmc/tech.html. M.E.L. is a bioinformatics advisor to Elysium Health. Y.L., N.D. and D.A.S. are inventors on patents arising from this work (WO/2020/069373 and WO/2020/069339), filed by the President and Fellows of Harvard College. The other authors declare no competing interests.

**Additional information**


**Supplementary information** is available for this paper at https://doi.org/10.1038/s41586-020-2975-4.



**Correspondence and requests for materials** should be addressed to D.A.S.



**Peer review information** *Nature* thanks Andrew Huberman, Hongjun Song, Yasuhiro Yamada and the anonymous reviewer(s) for their contribution to the peer review of this work. Peer reviewer reports are available.

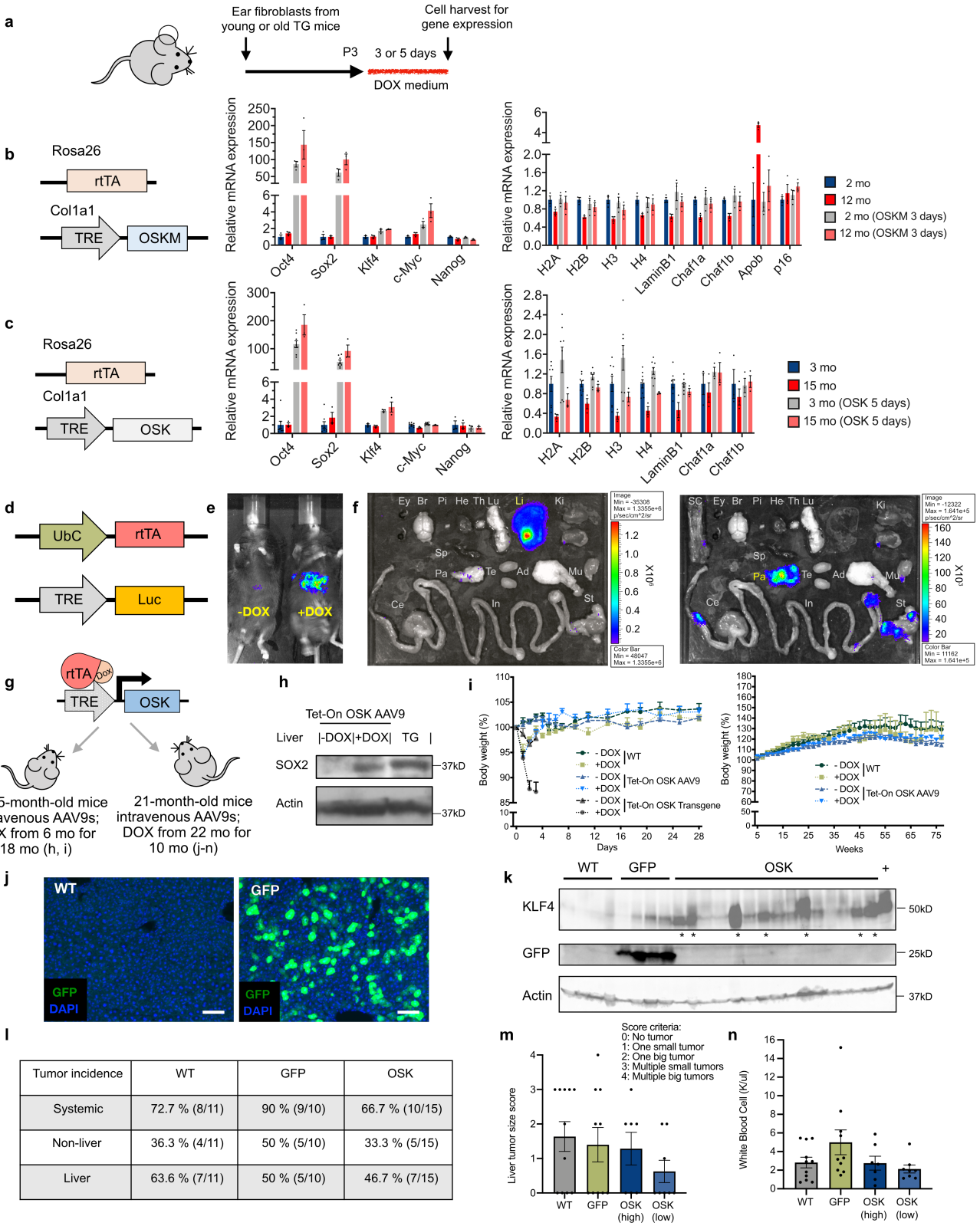


| Tumor incidence | WT | GFP | OSK |
|---|---|---|---|
| Systemic | 72.7 % (8/11) | 90 % (9/10) | 66.7 % (10/15) |
| Non-liver | 36.3 % (4/11) | 50 % (5/10) | 33.3 % (5/15) |
| Liver | 63.6 % (7/11) | 50 % (5/10) | 46.7 % (7/15) |

**Extended Data Fig. 1** | See next page for caption.

**Extended Data Fig. 1 | Effectiveness and safety of OSK reprogramming.** **a**, Experimental outline for testing the effects of OSKM and OSK on gene expression in fibroblasts from young and old transgenic (TG) mice. **b**, **c**, Expression of OSKM (**b**, $R26^{rtTA}$; $Col1a1^{OSKM}$, $n = 3$ biological replicates each condition) and OSK (**c**, $R26^{rtTA}$; $Col1a1^{OKS\text{-}mCherry}$, $n = 3$ and 8 biological replicates) rescue age-associated transcriptional changes without inducing *Nanog* mRNA. mo, month(s). qPCR primers are listed in Supplementary Table 7. **d**, AAV-ubiquitinC (UbC)-rtTA and AAV-TRE-Luc vectors for measuring tissue distribution. **e**, Luciferase imaging of WT mice 2 months after intravenous injection (retro-orbital) of AAV9-UbC-rtTA;TRE-Luc ($1.0 \times 10^{12}$ gene copies total). DOX was delivered in drinking water (1 mg $ml^{-1}$) for 7 days to +DOX mice. **f**, Luciferase imaging of the eye (Ey), brain (Br), pituitary gland (Pi), heart (He), thymus (Th), lung (Lu), liver (Li), kidney (Ki), spleen (Sp), pancreas (Pa), testis (Te), adipose (Ad), muscle (Mu), spinal cord (SC), stomach (St), small intestine (In) and caecum (Ce) 2 months after retro-orbital injection of AAV9-UbC-rtTA;TRE-Luc followed by treatment with DOX for 7 days. The luciferase signal was primarily in the liver. Imaging the same tissues with a longer exposure time (right) with the liver removed revealed a strong signal in the pancreas. **g**, Toxicity and safety studies in young and old mice after in vivo delivery of OSK-expressing AAVs. In **h**, **i**, at the age of 5 months, mice were intravenously injected with AAV9-rtTA;TRE-OSK (3 and $7 \times 10^{11}$ gene copies of AAV per mouse). After 1 month, mice remained untreated (−DOX) or were treated with DOX (+DOX) for 18 months. WT mice were not injected with AAV. In **j**–**n**, at the age of 21 months, mice were injected intravenously with $5 \times 10^{11}$ gene copies of AAV9-rtTA and $7 \times 10^{11}$ of either AAV9-TRE-GFP (GFP) or TRE-OSK (OSK) per mouse. After 1 month, GFP, OSK, and non-injected WT mice were treated with DOX for 10 months. **h**, SOX2 expression in the liver of WT mice 2 months after intravenous delivery of OSK-expressing AAV9s with or without a month of DOX induction, and in the liver of OSK transgenic mice, 129S1/C57BL/6J mixed background. Uncropped scans in are shown in Supplementary Fig. 1. **i**, Body weight of WT mice, OSK transgenic mice, and AAV-mediated OSK-expressing mice with or without DOX in the first 4 weeks (left; $n = 5, 3, 6, 4, 4$ and 3 mice) and after 17 months (right, $n = 5, 3, 6$ and 4 mice). **j**, Examples of liver sections from WT or GFP mice showing the infection of AAV9. Scale bar, 100 µm. **k**, KLF4 and GFP protein levels in the livers of WT, GFP and OSK mice at 32 months of age. * indicates high OSK expression, + indicates induced protein expression levels in livers of OSK transgenic mice. Uncropped scans are shown in Supplementary Fig. 1. **l**, Tumour incidence in WT, GFP, and OSK mice at age 32 months after 10 months of DOX induction. **m**, **n**, Liver tumour scores (**m**) and white blood cell counts (**n**) for WT, GFP and OSK groups at age 32 months after 10 months of DOX induction. OSK mice were defined as either high expression (indicated by * in **k**) or low expression (WT, $n = 11$ mice; GFP, $n = 10$ mice; OSK high, $n = 7$ mice; OSK low, $n = 8$ mice). For **m**, **n**, there was no difference between the groups using one-way ANOVA. All data are presented as mean ± s.e.m.

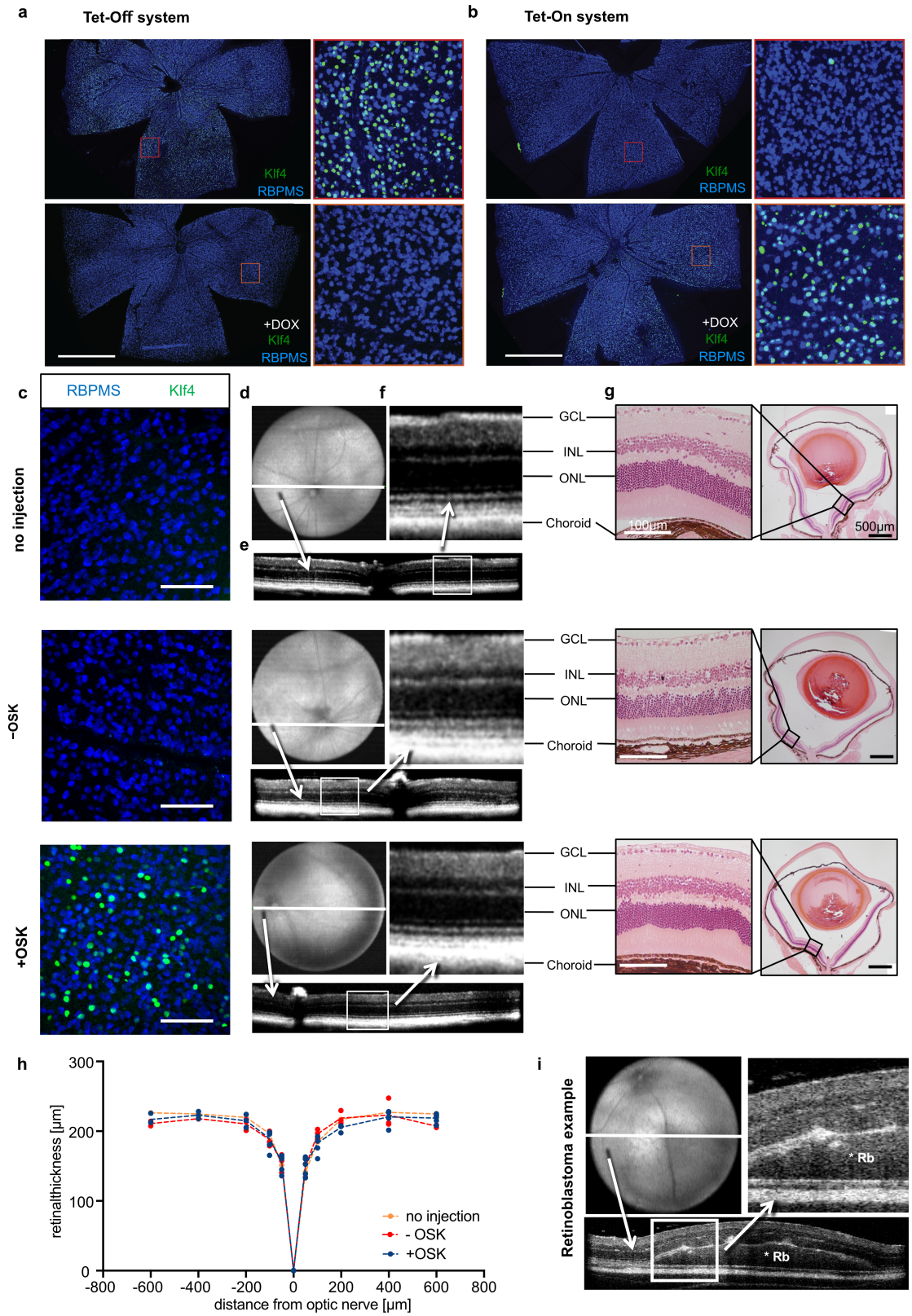


**Extended Data Fig. 2** | See next page for caption.

**Extended Data Fig. 2 | Normal architecture and absence of tumours in the retina after long-term OSK expression mediated by AAV2 delivery.** **a**, **b**, Representative wholemount retina display of RBPMS (a RGC marker) and *Klf4* immunofluorescence showing (**a**) expression from the AAV2 Tet-Off system can be turned off by DOX in drinking water (2 mg ml$^{-1}$, 3 days), and (**b**) expression from the AAV2 Tet-On system can be turned on by DOX (2 mg ml$^{-1}$, 2 days). Scale bars, 1 mm; $n = 4$ retinas for each condition. **c**, Corresponding retinal wholemount images stained for RBPMS and *Klf4* are shown for each group tested: top, no injection, $n = 6$; middle, −OSK (intravitreal injection of AAV2-rtTA;TRE-OSK without DOX induction), 10 months post-injection, $n = 3$; bottom, +OSK (intravitreal injection of AAV2-tTA;TRE-OSK with DOX induction), 15 months post-injection, $n = 6$. All retinas are from 16-month-old mice, showing similar expression within the group. Scale bars, 100 µm. **d**, Volume intensity projection of en-face OCT (optical coherence tomography) retinal image with a white line indicating the location of **e**. **e**, Representative retinal cross-section B-scan images. White box indicates the location of the high magnification scans in **f** (retinal layers: GCL, ganglion cell layer; INL, inner nuclear layer; ONL, outer nuclear layer and choroid). Videos of complete retinal cross-section B-scan images of the entire globe are provided as Supplementary Videos 1–3. **g**, Low- and high-power representative images of haemotoxylin and eosin (H&E)-stained cross-sections of corresponding eyes, verifying retinal layers. **h**, Quantitative measurements of retinal thickness, there was no difference between the groups at any location using two-way ANOVA with Bonferroni correction ($n = 6$, 3 and 6, respectively). **i**, Immunosuppressed NOD scid gamma mice received a subretinal injection of approximately 10,000 human retinoblastoma tumour cells. The OCT image shows a small retinal tumour and increased retinal thickness 14 days post-injection, demonstrating the ability of the OCT scan to detect tumours. *Rb indicates retinoblastoma.

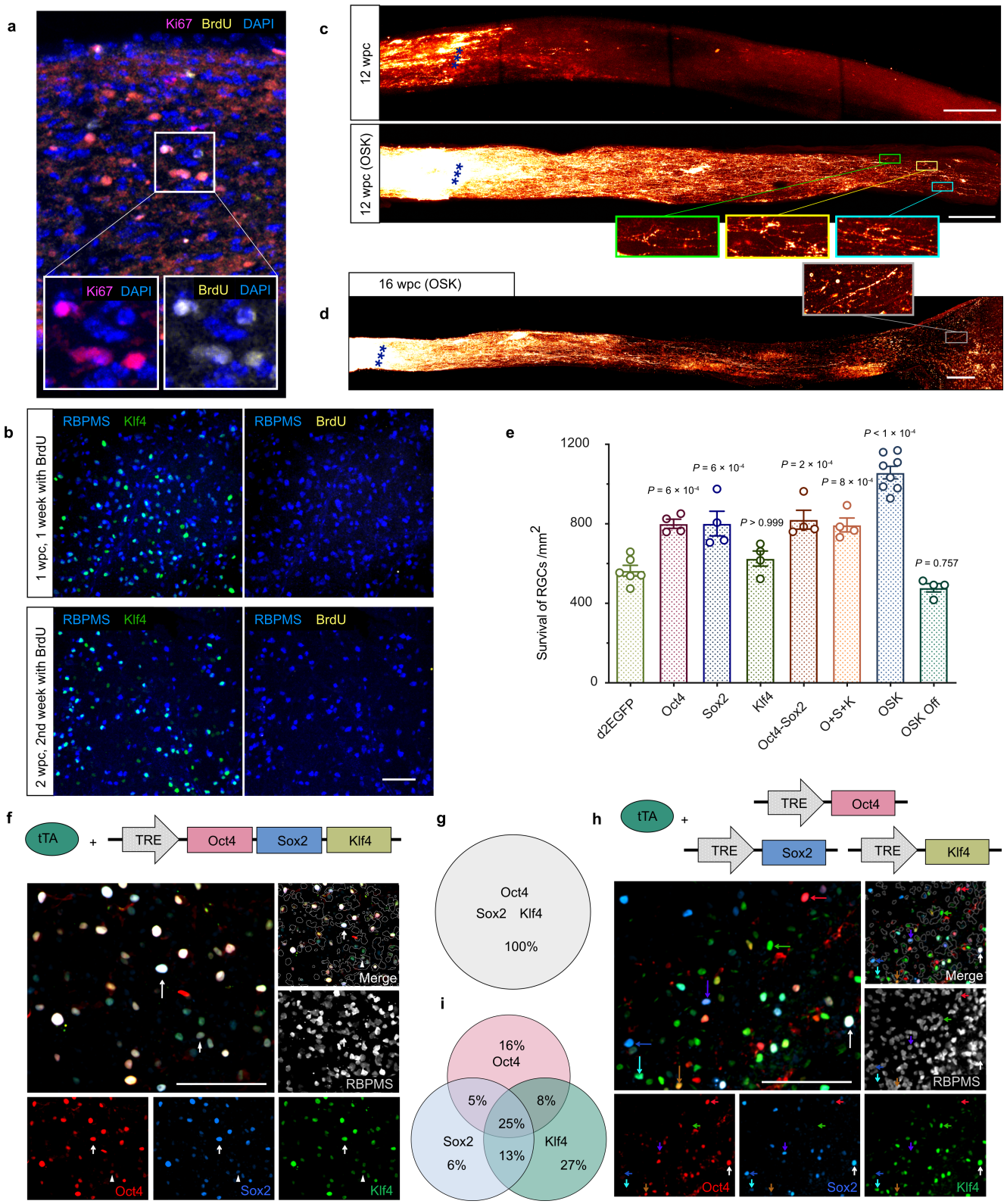


**Extended Data Fig. 3** | See next page for caption.

**Extended Data Fig. 3 | Polycistronic OSK induces long-distance axon regeneration post-injury without RGC proliferation. a**, Proliferating cells in the optic nerve (for example, glial cells) in BrdU-injected mice as a positive control ($n = 2$ nerves). BrdU staining co-localized with Ki67, a proliferation marker. **b**, Representative retina wholemount staining shows OSK-expressing RGCs do not stain for BrdU in the first or second week after crush injury; $n = 4$ retinas. Scale bars, 100 µm. **c**, Imaging of optic nerves showing regenerating and sprouting axons with or without OSK AAV treatment, 12 weeks post-crush (wpc); $n = 2$ nerves. Scale bars, 200 µm. **d**, Whole-nerve imaging showing CTB-labelled regenerative axons at 16 wpc in WT mice with intravitreal injection of AAV2-tTA;TRE-OSK ($n = 2$ nerves). Scale bars, 200 µm. **e**, Survival of RBPMS-positive cells in the RGC layer transduced with different AAV2s, 16 dpc ($n = 6, 4, 4, 4, 4, 4, 8$ and 4 eyes). All data are mean ± s.e.m. **f**, **g**, Representative immunofluorescence (**f**) and sub-population proportion (**g**) of wholemount retinas transduced with a polycistronic AAV vector expressing *Oct4*, *Sox2* and *Klf4* in the same cell. White arrows designate triple-positive cells. $n = 3$ retinas. Scale bars, 100 µm. **h**, **i**, Immunofluorescence (**h**) and sub-population proportion (**i**) of wholemount retinas transduced with AAVs separately encoding *Oct4*, *Sox2* and *Klf4*. Red, blue, and green arrows designate single-positive cells, with a white arrow marking a triple-positive cell, and other arrows marking double-positive cells. $n = 3$ retinas. Scale bar, 100 µm. One-way ANOVA with Bonferroni correction in **e**, with comparisons to d2EGFP shown.

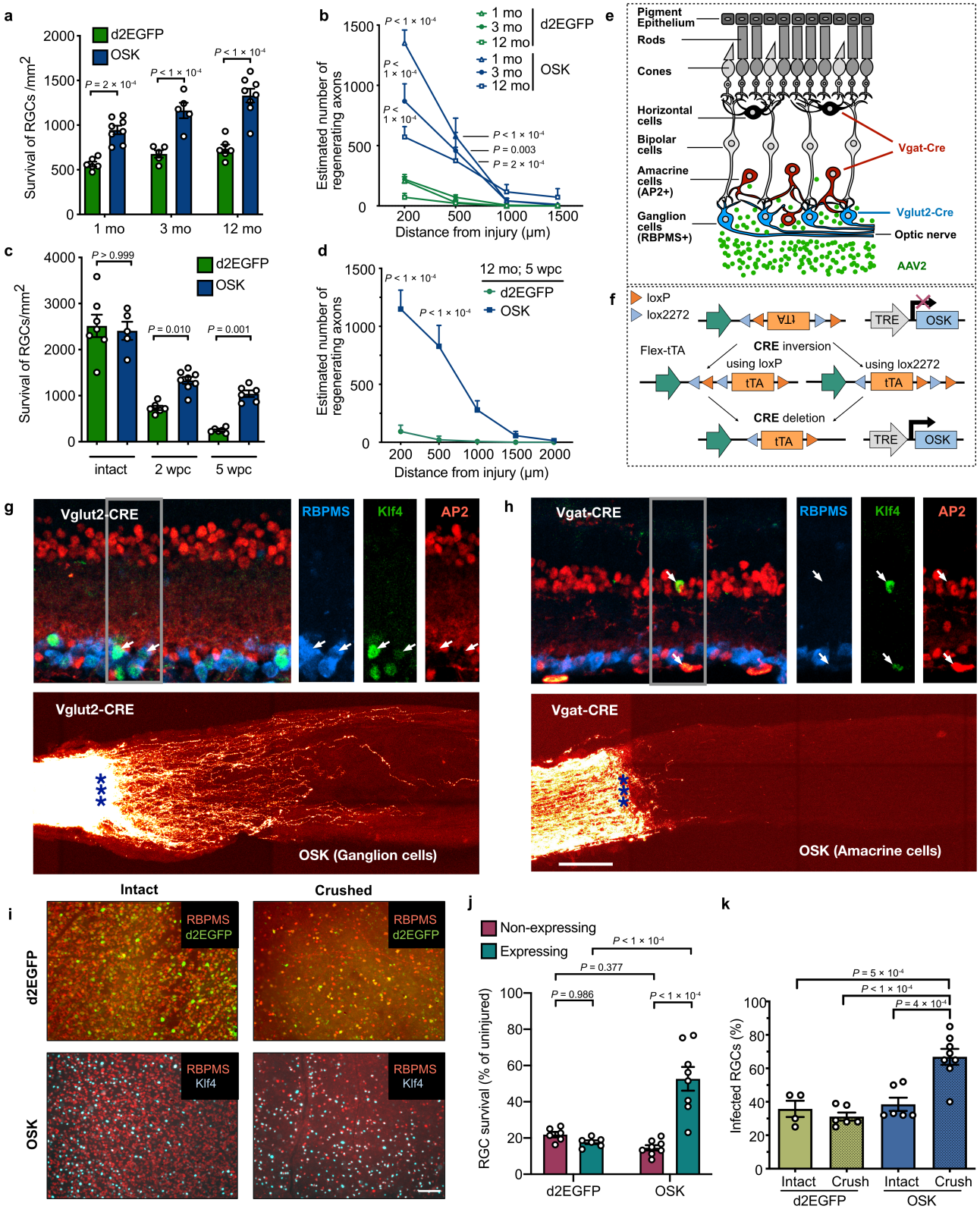


**Extended Data Fig. 4** | See next page for caption.

**Extended Data Fig. 4 | Regenerative and pro-survival effects of OSK are RGC-specific and cell-autonomous. a**, Effect of OSK expression on RGC survival in young (1-month-old, $n = 8$), adult (3-month-old, $n = 5$), and old (12-month-old, $n = 8$) mice after optic-nerve crush-injury compared to expression of d2EGFP as a negative control ($n = 6$, 5 and 6, respectively). **b**, Axon regeneration after OSK expression compared to d2EGFP controls in young (1-month-old, $n = 5$, 6), adult (3-month-old, $n = 6$), and old (12-month-old, $n = 4$, 5) mice, 2 wpc. **c**, Number of RGCs in the intact, 2 wpc or 5 wpc retinas of 12-month-old mice expressing GFP (AAV2-tTA;TRE-d2EGFP, $n = 7$, 6 and 6, respectively) or OSK (AAV2-tTA;TRE-OSK, $n = 5$, 8 and 6, respectively). **d**, Axon regeneration in 12-month-old mice with OSK AAV or control AAV (d2EGFP) treatment, 5 wpc ($n = 5$ nerves). **e**, Schematic of retinal structure showing Vglut2-Cre mice selectively expressing Cre in excitatory neurons such as RGCs, whereas Vgat-Cre mice selectively express Cre in inhibitory amacrine and horizontal cells. **f**, Schematic of the FLEx (flip-excision) Cre-switch system. AAV2-FLEx-tTA is inverted by Cre to express tTA and therefore induces OSK only in Cre-positive cells. **g**, Confocal image stack demonstrating delivery of AAV2-FLEx-tTA;TRE-OSK to intact Vglut2-Cre transgenic retinas, resulting in RGC-specific OSK expression (top) and robust axon regeneration in the optic nerve (bottom). White arrows indicate RBPMS+ (AP2-)-labelled RGCs that express *Klf4* (green). $n = 4$ independent replicates. **h**, Confocal image stack demonstrating delivery of AAV2-FLEx-tTA;TRE-OSK to intact Vgat-Cre transgenic retinas, resulting in amacrine-specific OSK expression (top) and poor axon regeneration in the optic nerve (bottom). White arrows indicate AP2+ (RBPMS-)-labelled amacrine cells that express *Klf4* (green). $n = 4$ independent replicates. **i**, Representative image of AAV-expressing or non-expressing RGCs in intact and crushed retinas 2 wpc with AAVs expressing d2EGFP or OSK. d2EGFP: AAV2-tTA;TRE-d2EGFP, $n = 6$ retinas; OSK: AAV2-tTA;TRE-OSK, $n = 8$ retinas. **j**, RGC survival rate (crushed/intact) of d2EGFP- ($n = 6$ eyes) or *Klf4*-expressing cells ($n = 8$ eyes) and their surrounding non-expressing cells indicating a cell-autonomous pro-survival effect of OSK-expressing RGCs after crush, 2 wpc. **k**, Frequency of d2EGFP- or *Klf4*-positive RGCs pre- or 2 weeks post-injury ($n = 4$, 6, 6 and 8 eyes). Two-way ANOVA with Bonferroni correction in **a**–**d**, **j**; one-way ANOVA with Bonferroni correction in **k**. Scale bars (**g**–**i**), 100 µm. All data are mean ± s.e.m.

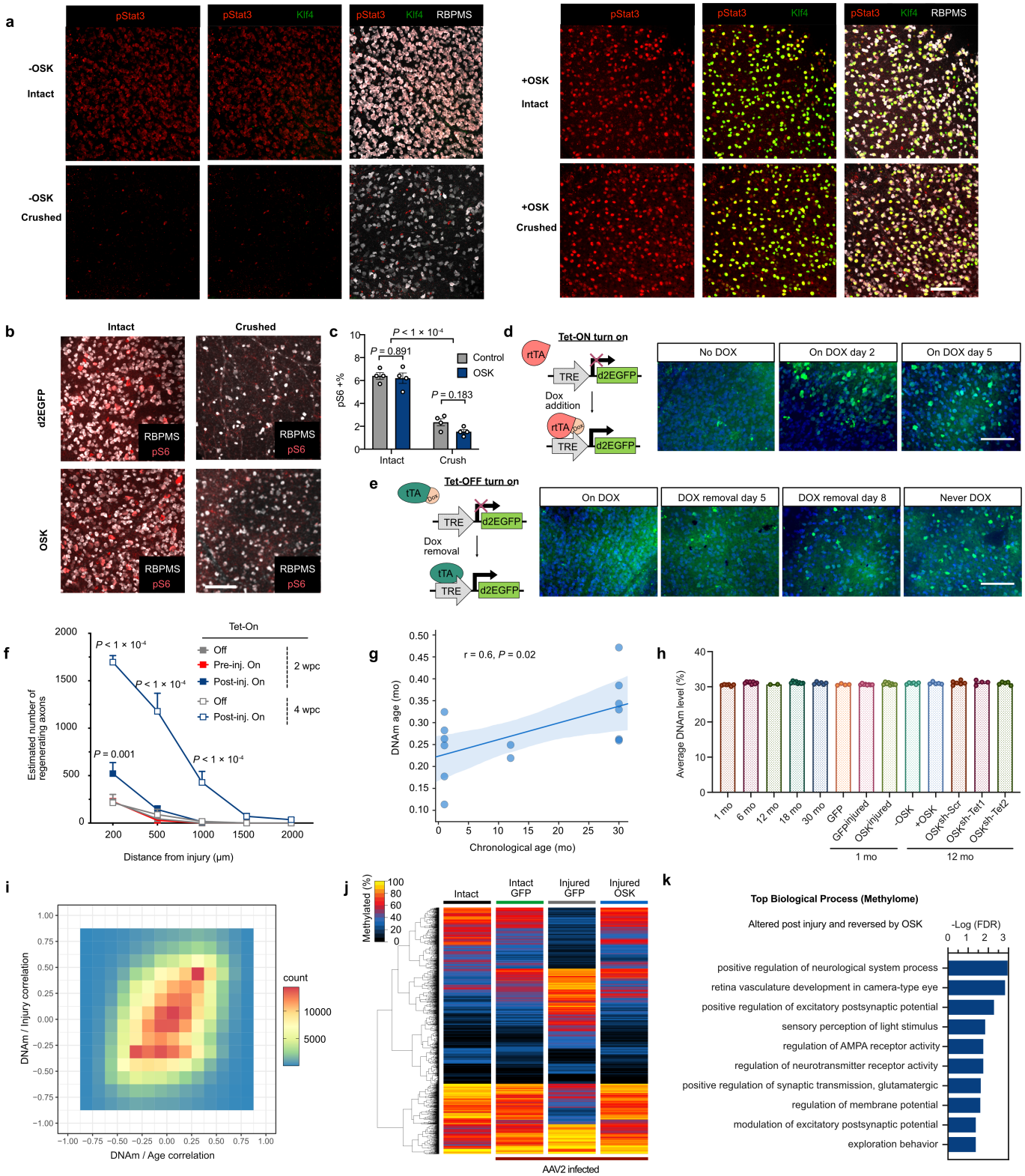


**Extended Data Fig. 5** | See next page for caption.

**Extended Data Fig. 5 | OSK activates *Stat3* in the absence of mTOR activation or global demethylation. a**, Representative images of retinal wholemounts transduced with AAV2-tTA (−OSK) or AAV2-tTA;TRE-OSK (+OSK) in the presence or absence of crush injury after 3 days. Retinal wholemounts immunostained for *pStat3*, *Klf4* and RBPMS. $n = 2$ retinas each condition. **b**, Representative images of retinal wholemounts transduced with d2EGFP- or OSK-encoding AAV2 in the presence or absence of a crush injury. Retinal wholemounts immunostained for RBPMS and mTOR activation marker phosphorylated S6 (pS6). $n = 4$ retinas for each condition. **c**, Percentage of pS6-positive RGCs in intact and crushed samples ($n = 4$ retinas for each condition). **d**, Representative images of d2EGFP in retina expressed from the Tet-On AAV system. No GFP expression was observed in the absence of DOX. GFP expression reached peak levels 2 days after DOX induction and remained at a similar level at day 5 after induction. $n = 2$ retinas each condition. **e**, Representative images of retinal d2EGFP expression using the Tet-Off AAV system with various durations of DOX treatments (2 mg ml$^{-1}$). Once pre-treated with DOX to suppress expression (on DOX), GFP was sparse even on day 8 after DOX withdrawal, lower than peak expression (Never DOX). $n = 2$ retinas each condition. **f**, Axon regeneration at 2 or 4 wpc in response to OSK induction either pre- or post-injury ($n = 4, 5, 5, 4$ and 4 eyes, respectively). **g**, Correlation between ribosomal DNA methylation (DNAm) age and chronological age of sorted mouse RGCs (1 month, $n = 6$; 12 months, $n = 2$; 30 months, $n = 5$), with the light blue region representing the confidence interval. *P* value of the linear regression is calculated by two-sided *F*-test of overall significance. In agreement with previous studies, DNA methylation age estimates of neurons tend to be lower than their chronological age but remain correlated (see Methods). **h**, Average DNA methylation levels across the mouse genome in RGCs from different ages and treatments, based on 703,583 shared CpG sites from RRBS of all samples (combined strands), $n = 6, 8, 2, 8, 6, 4, 8, 8, 6, 5, 6, 4$ and 5, respectively. **i**, Correlation of DNA methylation at each CpG site versus age (*x*-axis; 1 month, 12 months, 30 months) and versus injury (*y*-axis; intact, injured GFP). The heat map represents the number of sites located in each block of value coordinates. Pearson's correlation coefficient, $r = 0.34$, $P < 1e^{-200}$. **j**, Hierarchical clustered heat map of methylation levels of 4,106 CpGs that significantly changed in RGCs after crush injury (intact vs injured GFP, $q < 0.05$) and the effect of OSK. **k**, Top biological processes associated with the 698 CpGs that were significantly altered by both injury and OSK. Two-way ANOVA with Bonferroni correction in **c**, **f**. Scale bars (**a**, **b**, **d**, **e**), 100 µm. All data are mean ± s.e.m.

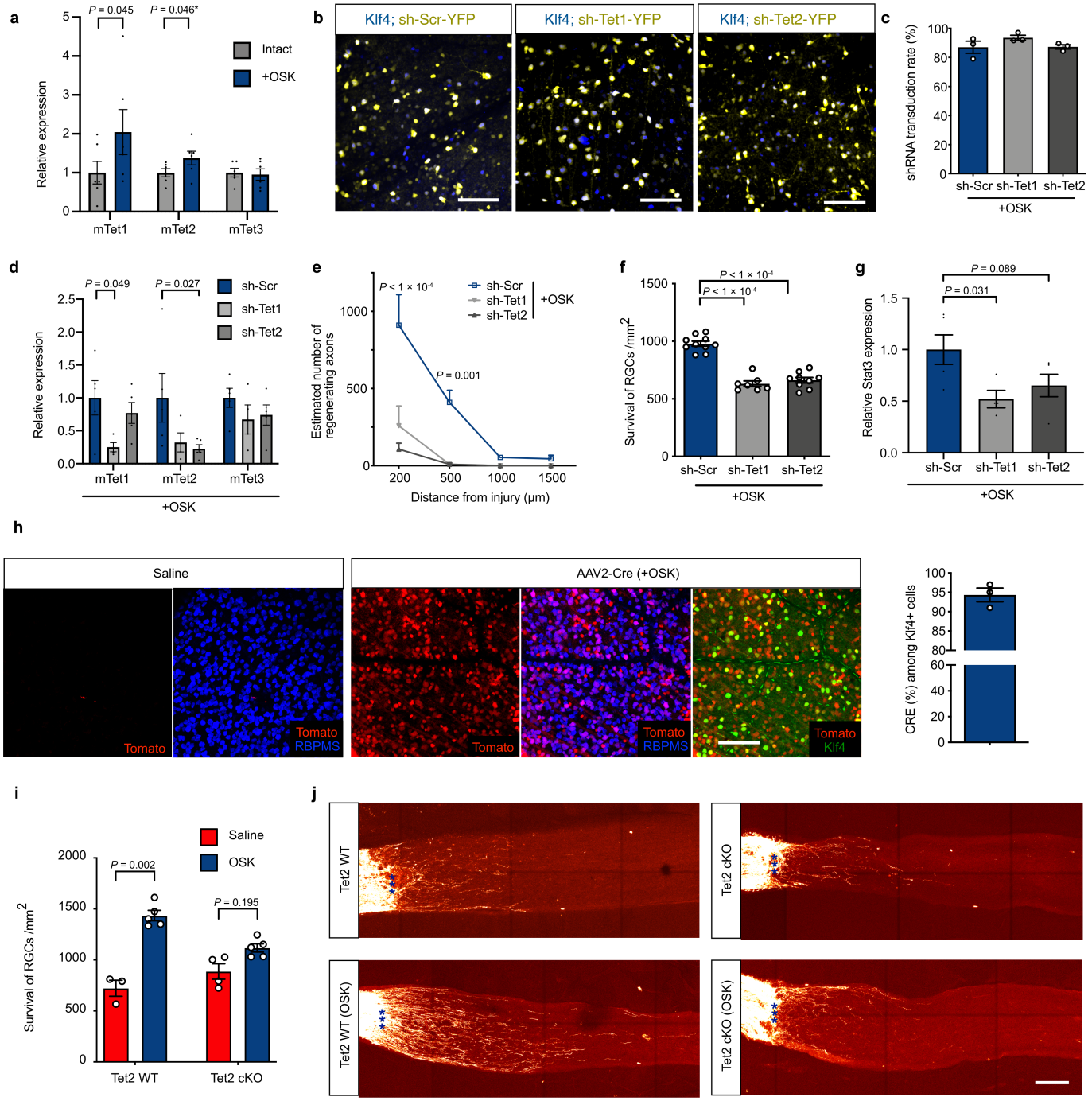


**Extended Data Fig. 6 | Protective and regenerative effect of OSK is dependent on TET1 and TET2. a**, Mouse *Tet1*, *Tet2* and *Tet3* mRNA levels with or without OSK expression in RGCs ($n = 6$ biological replicates each condition). The *P* value indicated with an asterisk was calculated using an unpaired one-tailed *t*-test. **b**, Representative images of retinal wholemounts transduced with AAV2-tTA;TRE-OSK in combination with a AAV2-shRNA-YFP (yellow fluorescent protein) having either a scrambled sequence (sh-Scr) or a hairpin sequence to knockdown *Tet1* (sh-Tet1) or *Tet2* (sh-Tet2) expression, at titre ratio 5:5:1. Retinal wholemounts immunostained for *Klf4*. $n = 3$ retinas for each condition. **c**, Quantification of shRNA-YFP AAV transduction in OSK-expressing RGCs ($n = 3$ retinas for each condition). **d**, Mouse *Tet1*, *Tet2* and *Tet3* mRNA levels with sh-Scr ($n = 5$), sh-Tet1 ($n = 4$) or sh-Tet2 ($n = 5$) YFP AAV2 in RGCs in the presence of OSK expression. **e**, **f**, Quantification of axon regeneration (**e**, $n = 4$ eyes each condition) and RGC survival (**f**, $n = 10$, 7 and 9 eyes) at 2 wpc in retinas co-transduced with AAV2- tTA;TRE-OSK;shRNA. **g**, Mouse *Stat3* mRNA levels after knockdown using sh-Scr ($n = 5$), sh-Tet1 ($n = 4$) or sh-Tet2 ($n = 5$) in RGCs in the presence of OSK expression. **h**, Cre-dependent Tomato expression in RGCs after intravitreal AAV2-Cre injection of Tomato reporter mice (Rosa-CAG-lox-STOP-lox-Tomato), and the co-expressed frequency of Cre and *Klf4* ($n = 3$ eyes). **i**, **j**, RGC survival (**i**) and representative longitudinal sections of regenerating axons in longitudinal sections (**j**) in response to OSK expression (AAV2-tTA;TRE-OSK, $n = 5$ for each condition) compared to no expression (saline, $n = 3$ and 4), 16 days after crush injury in *Tet2*$^{flox/flox}$ mice injected with saline (Tet2 WT) or AAV2-Cre (Tet2 cKO). Scale bars (**b**, **h** and **j**), 100 μm. Two-way ANOVA in **a**, **d**, **i**; unpaired two-tailed Student's *t*-test in **g**; one-way ANOVA in **e**, **f**. All data are mean ± s.e.m.

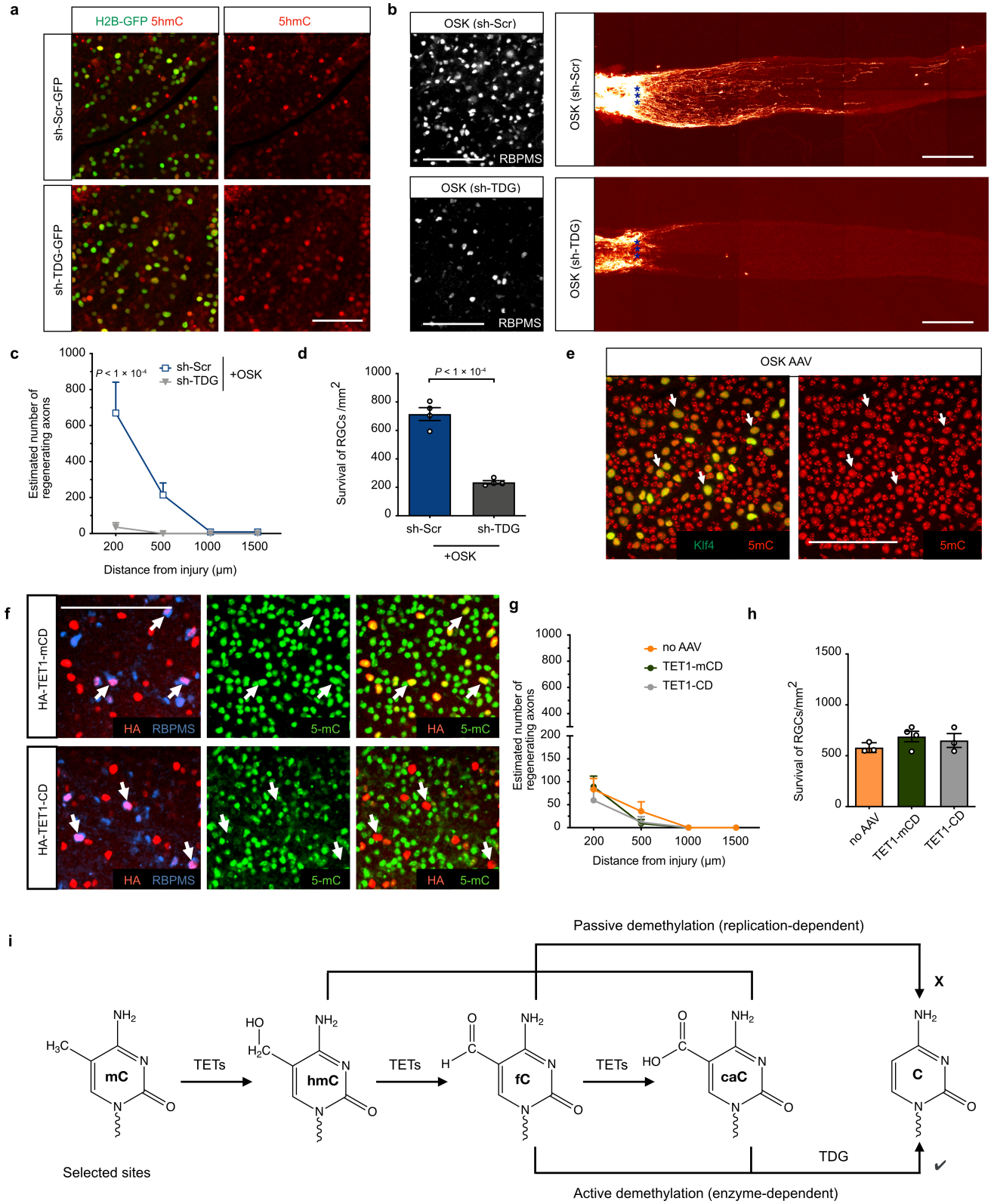


**Extended Data Fig. 7** | See next page for caption.

**Extended Data Fig. 7 | OSK-induced axon regeneration and survival require non-global active DNA demethylation through thymine DNA glycosylase.** **a**, Representative images of retinal wholemounts transduced with sh-Scr-H2B-GFP or sh-TDG-H2B-GFP AAV2 s for 4 weeks, demonstrating that knockdown of thymine DNA glycosylase (TDG) increased levels of 5-hydroxymethylcytosine (5-hmC). $n = 4$ retinas for each condition. **b**, Representative retinal wholemount images and images of longitudinal sections through the optic nerve showing CTB-labelled regenerative axons in WT mice, 16 dpc after an intravitreal injection of AAV2-tTA ;TRE-OSK in combination with AAV2-sh-Scr (sh-Scr) or AAV2-sh-TDG (sh-TDG) at titre ratio 5:5:1. $n = 4$ retinas for each condition. **c**, **d**, Quantification of regenerating axons (**c**) and RGC survival (**d**) in OSK-treated mice 16 dpc with AAVs carrying sh-Scr or sh-TDG ($n = 4$ nerves for each condition). **e**, Representative image of retinal wholemounts transduced with AAV2-tTA;TRE-OSK. Retinal wholemounts were immunostained for 5-methylcytosine (5-mC) and *Klf4*, showing a lack of global demethylation in OSK expressing RGCs. $n = 3$ retinas. **f**, Representative images of retinal wholemounts transduced with AAV2 vectors encoding the HA-TET1 catalytic domain (TET1-CD) or its catalytic mutant (TET1-mCD) for 4 weeks, demonstrating that overexpression of TET1-CD decreases global 5-mC levels. $n = 3$ retinas for each condition. **g**, **h**, Quantification of axon regeneration (**g**) and RGC survival (**h**) at 2 wpc in retinas transduced without or with AAV2 vectors encoding HA-TET1 CD mutant or HA-TET1 CD ($n = 3$, 4 and 3 eyes). **i**, A schematic diagram illustrating passive demethylation and TDG-dependent active DNA demethylation. Scale bars (**a**, **b**, **e**, **f**), 100 µm. One-way ANOVA with Bonferroni's multiple comparison test in **c**, **g**, **h**; unpaired two-tailed Student's *t*-test in **d**. There was no difference between the groups in **g** and **h** using two-way ANOVA and one-way ANOVA, respectively. All data are mean ± s.e.m.

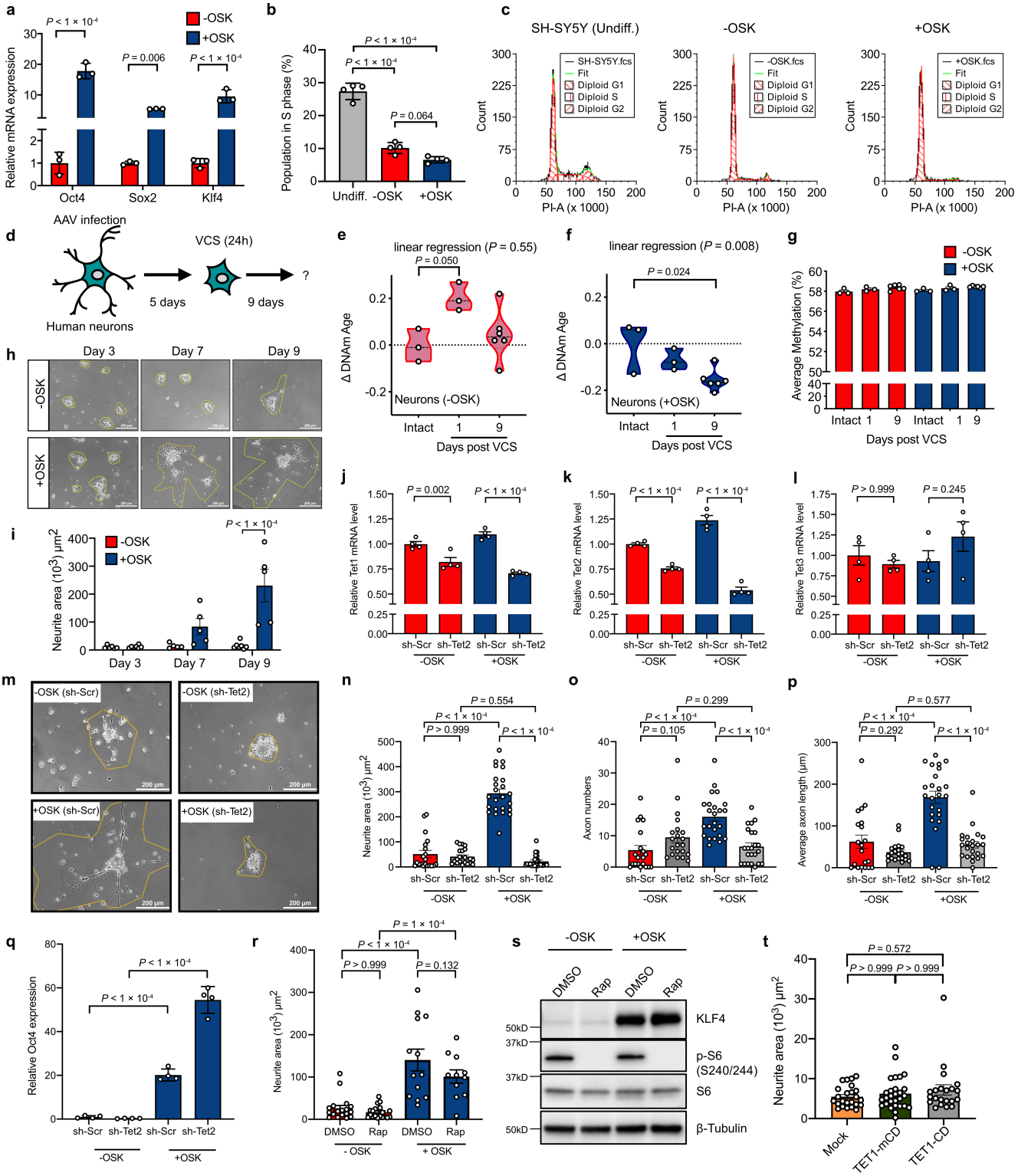


**Extended Data Fig. 8** | See next page for caption.

**Extended Data Fig. 8 | OSK induces axon regeneration and reversal of DNA methylation age in human neurons. a**, mRNA levels of mouse *Oct4*, *Sox2* and *Klf4* in human neurons transduced with vectors packaged by AAV-DJ, a recombinogenic hybrid capsid that is efficient for in vitro transduction. −OSK: AAV-DJ-tTA ($n = 3$); +OSK: AAV-DJ-tTA;TRE-OSK ($n = 3$). **b**, Percentage of cells in S phase, as measured by propidium iodide (PI)-staining ($n = 4$). **c**, FACS profiles of G1, S and G2 phases in undifferentiated SH-SY5Y cells and differentiated cells transduced with −OSK and +OSK vectors. **d**, Experimental outline for testing axon regeneration in human neurons after vincristine (VCS) damage. **e**, **f**, DNA methylation (DNAm) age of human neurons without damage (intact), and 1 or 9 days after VCS damage in the absence (**e**) or presence (**f**) of OSK expression, measured using the skin and blood clock suited to in vitro studies (see Methods). The linear regression *P* value in **e** ($P = 0.55$) indicates nonlinear DNA methylation age changes, and in **f** ($P = 0.008$) indicates a continuous decrease in DNA methylation age ($n = 3$, 3 and 6). **g**, Average DNA methylation levels among 850,000 probes from the EPIC array in human neurons without damage (intact), and 1 or 9 days after VCS damage in the absence or presence of OSK expression ($n = 3$, 3 and 6). **h**, **i**, Representative images (**h**, similar results were confirmed in two series of experiments) and quantification (**i**) of neurite area at different time points after VCS damage ($n = 6$, 7, 5, 5, 7 and 5; 2 independent experiments). Cells were not passaged after damage to avoid cell–cell contact for quantifying maximum axon regeneration. **j**–**l**, Human *TET1*, *TET2* and *TET3* mRNA level with scrambled shRNA (sh-Scr) or sh-Tet2 AAV in human neurons in the presence or absence of OSK expression ($n = 4$; 2 independent experiments). **m**, Representative images of human neurons in each AAV treated group, 9 days after VCS damage. Similar results were confirmed in three series of experiments. **n**–**p**, Neurite area (**n**), axon number (**o**) and axon length (**p**) in each AAV-treated group 9 days after VCS damage ($n = 20$, 21, 24 and 23; 3 independent experiments). **q**, Mouse *Oct4* mRNA levels (from OSK AAV) in human neurons with sh-Scr or sh-Tet2 AAV and in presence or absence of OSK AAV ($n = 4$). **r**, The effect of mTOR inhibition by rapamycin (Rap, 10 nM) on axon regeneration of differentiated neurons with or without OSK ($n = 18$, 19, 13 and 11; 2 independent experiments). **s**, S6 phosphorylation levels in human neurons 5 days after treatment with rapamycin (Rap, 10 nM). Similar results were seen in two independent experiments. Uncropped scans are shown in Supplementary Fig. 1. **t**, Neurite area of neurons expressing TET1 catalytic domain (TET1-CD) or its catalytic mutant (TET1-mCD) 9 days after VCS damage ($n = 24$, 28 and 21; 2 independent experiments). One-way ANOVA with Bonferroni's multiple comparison test in **b**, **e**–**g** and **t**; two-way ANOVA with Bonferroni's multiple comparison test in **a**, **i**, **j**–**l** and **n**–**r**. All bar graphs are mean ± s.e.m.

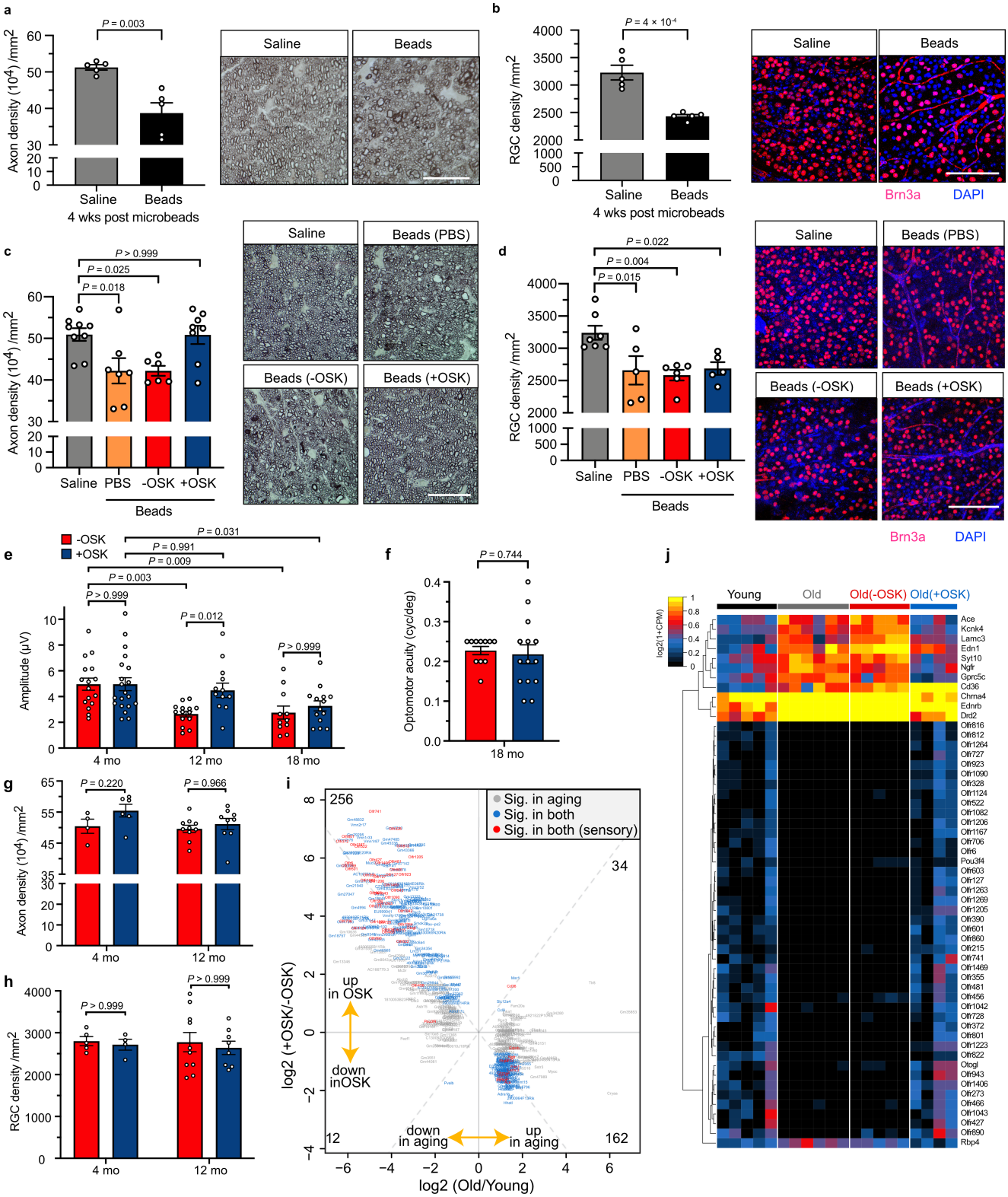


**Extended Data Fig. 9** | See next page for caption.

**Extended Data Fig. 9 | Vision restoration and regenerative effect of OSK rely on functional improvement of existing RGCs. a**, Axon density and representative photomicrographs of PPD-stained optic nerve cross-sections, 4 weeks after microbead or saline injection (baseline, $n = 5$ eyes each condition). Scale bars, 25 µm. **b**, Quantification of RGCs and representative confocal microscopic images from retinal flat-mounts stained with anti-Brn3a (red), an RGC-specific marker, and DAPI (4′,6-diamidino-2-phenylindole, blue), a nuclear stain, 4 weeks after microbead or saline injection (baseline, $n = 5$ eyes each condition). Scale bar, 100 µm. **c**, Axon density and representative micrographs from PPD-stained optic nerve cross-sections, 4 weeks after AAV2 or PBS injection (treated, $n = 9, 7, 6$ and 8 eyes). Scale, 50 µm. **d**, Quantification of RGCs and representative confocal microscopic images 4 weeks after PBS or AAV injection (treated, $n = 7, 5, 6$ and 5 eyes). Scale bar, 100 µm. **e**, PERG measurement at different ages 4 weeks after −OSK ($n = 16, 14$ and 11 eyes) or +OSK treatment ($n = 20, 12$ and 14 eyes). Similar results from 2 independent experiments are combined. **f**, Visual acuity in 18-month-old mice treated with −OSK ($n = 11$ eyes) or +OSK ($n = 14$ eyes) AAV for 4 weeks. **g**, **h**, Axon (**g**; $n = 4, 6, 10$ and 9 nerves) and RGC (**h**; $n = 5, 4, 10$ and 8 retinas) density in 4- and 12-month-old-mice, 4 weeks after −OSK or +OSK AAV injection. **i**, Scatter plot of OSK-induced changes and age-associated changes in mRNA levels in RGCs, with differentially expressed genes labelled. Gene selection criteria are in Methods. **j**, Hierarchical clustered heat map showing relative mRNA levels of age-associated sensory perception genes in FACS-sorted RGCs from untreated young (5-month-old) or old (12-month-old) mice or old mice treated with either −OSK or +OSK AAV. Sensory genes were extracted from the mouse Sensory Perception (GO:0007600) category of the Gene Ontology database. Gene selection criteria are in Methods. −OSK: AAV2-rtTA;TRE-OSK for **c**–**h**, AAV2-TRE-OSK for **i**, **j**; +OSK: AAV2-tTA;TRE-OSK for **c**–**j**. Unpaired two-tailed Student's *t*-test in **a**, **b**, **f**; one-way ANOVA with Bonferroni's multiple comparison test in **c**, **d**; two-way ANOVA with Bonferroni correction in **e**, **g**, **h**. All data are mean ± s.e.m.

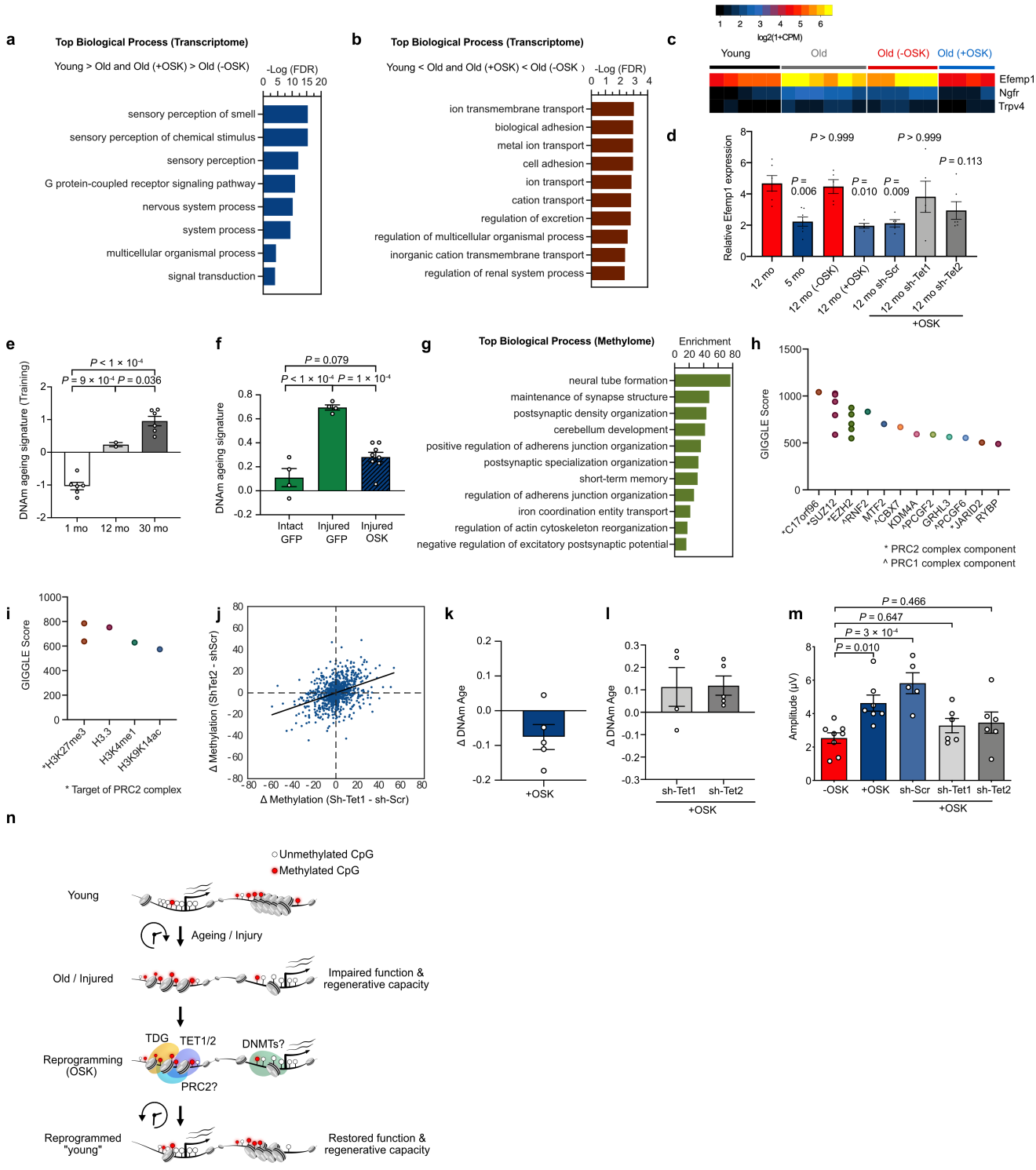


**Extended Data Fig. 10** | See next page for caption.

**Extended Data Fig. 10 | OSK expression in old RGCs restores youthful epigenetic signatures. a**, **b**, Top biological processes based on transcriptome data that were either lower expressed in old compared to young RGCs and reversed by OSK (**a**), or higher expressed in old RGCs compared to young and reversed by OSK (**b**). **c**, Heat map showing relative mRNA levels of genes involved in the negative regulation of neural projection development, among the 464 differentially expressed genes during ageing. The accumulation of the gene *Efemp1* during ageing is suspected to have a role in diseases of the retina. **d**, RGC *Efemp1* mRNA levels measured by qPCR (relative to GAPDH) compared between young mice, old mice, and old mice treated with −OSK or +OSK AAV. Old RGCs with sh-Scr, sh-Tet1 or sh-Tet2 knockdown combined with +OSK AAV are included for comparison ($n = 7, 6, 5, 4, 5, 5$ and 6 eyes). **e**, Principal component 1 value of 1 month, 12 month and 30 month RGC training samples in the PCA analysis. Values are standardized to have a mean = 0 and s.d. = 1 ($n = 6$, 2 and 6). **f**, DNA methylation ageing signatures of 6-week-old RGCs isolated from axon-intact retinas infected with GFP-expressing AAV, or from axon-injured retinas infected with GFP- or OSK- expressing AAV at 4 dpc ($n = 4, 4$ and 8 eyes). **g**, Top biological processes associated with the 1,226 signature CpG sites. **h**, **i**, Transcription factor (TF) binding (**h**) and histone modifications (**i**) specifically enriched at the 1,226 signature CpG sites, compared to five sets of randomly selected CpGs. **j**, Correlation of *Tet1* and *Tet2* knockdown-induced changes in methylation (5-mC and 5-hmC together) at the selected CpGs. $r = 0.4$, $P = 2.53e^{-45}$. **k**, Delta value of ribosomal DNA methylation age (months) of 12-month-old RGCs infected for 4 weeks with +OSK ($n = 5$ retinas). Values are relative to the average of RGCs infected with −OSK AAV. **l**, Ribosomal DNA methylation age (months) of 12-month-old OSK-treated RGCs infected for 4 weeks with sh-Tet1 or sh-Tet2 ($n = 4, 5$ retinas). Values are relative to the average of RGCs infected with sh-Scr. **m**, PERG amplitudes in old (12-month-old) mice treated with −OSK, +OSK or +OSK together with either sh-Scr or sh-Tet1/sh-Tet2-mediated knockdown for 4 weeks ($n = 8, 7, 5, 6$ and 6 eyes). **n**, Working model. The loss of youthful epigenetic information during ageing and injury (including genome-wide changes to DNA methylation, acceleration of the DNA methylation clock, and disruption of youthful gene expression patterns) causes a decline in tissue function and regenerative capacity. OSK-mediated reprogramming recovers youthful epigenetic information, reverses the DNA methylation clock, restores youthful gene expression patterns, and improves tissue function and regenerative capacity, a process that requires active DNA demethylation by TET1/TET2 and TDG. The PRC2 complex may serve to recruit TET1 and TET2 to specific sites in the genome, and DNA methylation by DNA methyltransferases (DNMTs) may be important as well. One-way ANOVA with Bonferroni's multiple comparison test in **d**–**f**, **m**. All data are mean ± s.e.m.

nature research

Corresponding author(s): David Sinclair

Last updated by author(s): Oct 6, 2020

# Reporting Summary

Nature Research wishes to improve the reproducibility of the work that we publish. This form provides structure for consistency and transparency in reporting. For further information on Nature Research policies, see Authors & Referees and the Editorial Policy Checklist.

## Statistics

For all statistical analyses, confirm that the following items are present in the figure legend, table legend, main text, or Methods section.

| n/a | Confirmed | |
|---|---|---|
| ☐ | ☒ | The exact sample size (*n*) for each experimental group/condition, given as a discrete number and unit of measurement |
| ☐ | ☒ | A statement on whether measurements were taken from distinct samples or whether the same sample was measured repeatedly |
| ☐ | ☒ | The statistical test(s) used AND whether they are one- or two-sided<br>*Only common tests should be described solely by name; describe more complex techniques in the Methods section.* |
| ☐ | ☒ | A description of all covariates tested |
| ☐ | ☒ | A description of any assumptions or corrections, such as tests of normality and adjustment for multiple comparisons |
| ☐ | ☒ | A full description of the statistical parameters including central tendency (e.g. means) or other basic estimates (e.g. regression coefficient) AND variation (e.g. standard deviation) or associated estimates of uncertainty (e.g. confidence intervals) |
| ☐ | ☒ | For null hypothesis testing, the test statistic (e.g. *F*, *t*, *r*) with confidence intervals, effect sizes, degrees of freedom and *P* value noted<br>*Give P values as exact values whenever suitable.* |
| ☒ | ☐ | For Bayesian analysis, information on the choice of priors and Markov chain Monte Carlo settings |
| ☒ | ☐ | For hierarchical and complex designs, identification of the appropriate level for tests and full reporting of outcomes |
| ☐ | ☒ | Estimates of effect sizes (e.g. Cohen's *d*, Pearson's *r*), indicating how they were calculated |

*Our web collection on statistics for biologists contains articles on many of the points above.*

## Software and code

Policy information about availability of computer code

| | |
|---|---|
| Data collection | For immunostaining imaging: Zeiss LSM 710 Multiphoton Laser Scanning Confocal, Leica TCS SP5 confocal microscope (Leica Microsystems) and Nikon 80i with Neurolucida and StereoInvestigator<br>For axon cross section: Nikon microscope (Eclipse E800, Nikon, Japan) with the DP Controller v. 1.2.1.108 and the DP Manager v. 1.2.1.107 software (Olympus)<br>For PERG: Celeris, Full-Field and Pattern Stimulation for the rodent model<br>For RT-qPCR: LightCycler 480 thermocycler (Roche)<br>For RNAseq and RRBS: sequenced using on the Illumina Hiseq2500/4000 |
| Data analysis | Statistical analyses were performed using GraphPad Prism 7/8 (GraphPad Software Inc., La Jolla, CA).<br>For images: ImageJ Fiji, version 2.0.0-rc- 69/1.52n)<br>For RNA-Seq analysis: R software version 3.4.2; edgeR R package version 3.26; hisat2 v2.1.0; featureCounts v1.6.4; AmiGO v2.5.12<br>For DNA methylation analysis: trim galore v0.4.1; Bismark v0.15.0 |

For manuscripts utilizing custom algorithms or software that are central to the research but not yet described in published literature, software must be made available to editors/reviewers. We strongly encourage code deposition in a community repository (e.g. GitHub). See the Nature Research guidelines for submitting code & software for further information.

## Data

Policy information about availability of data

All manuscripts must include a data availability statement. This statement should provide the following information, where applicable:

- Accession codes, unique identifiers, or web links for publicly available datasets
- A list of figures that have associated raw data
- A description of any restrictions on data availability

RRBS data for DNA methylation analysis and RNA-seq data are available in the Biosample database (NCBI) and under BioProject PRJNA655981. Illumina Human Methylation EPIC array data is available in the GEO database (NCBI) and under GSE147436. Associated figures are Fig. 2d and e, Fig. 4c-e, Extended Data Fig. 5g-k,

Extended Data Fig. 8e-g, Extended Data Fig. 9i, j, Extended Data Fig. 10a-c and e-l. All other relevant data that support the findings of this study are available from the corresponding author upon reasonable request.

# Field-specific reporting

Please select the one below that is the best fit for your research. If you are not sure, read the appropriate sections before making your selection.

☒ Life sciences ☐ Behavioural & social sciences ☐ Ecological, evolutionary & environmental sciences

For a reference copy of the document with all sections, see nature.com/documents/nr-reporting-summary-flat.pdf

# Life sciences study design

All studies must disclose on these points even when the disclosure is negative.

| | |
|---|---|
| Sample size | Although no statistical methods were used to predetermine sample size, we took into account former publications of the group (Parker, et al, 2008, Science; Sun, et al, Nature, 2011; Krishnan, et al, J Immunol, 2016; Bei, et al, Cell, 2016), to estimate the number of animals needed in each experiment (e.g., n = 4-7 for optic nerve crush study, n=5-20 for elevated IOP model and optomotor). |
| Data exclusions | (1) Mice that had intravitreal bleeding or developed signs of inflammation (clouding or an edematous cornea) during or post intravitreal injection were excluded from vision test and further histological analysis, exclusion criteria were pre-determined before the experiments;<br>(2) Optic nerves broken during dissection were not processed for accessing axon regeneration;<br>(3) Retinas infected with AAV2-tTA; TRE-d2EGFP were assessed for GFP signal during FACS and 1 sample that failed to show GFP signal was excluded from the group (Fig. 2d). |
| Replication | For in vivo experiments using rodent, biological replicates and independent cohorts of mice were used; for in vitro experiments, biological replicates as well as technical triplicates were used to ensure reproducibility. All attempts at replication were successful. |
| Randomization | The mice were randomly assigned into different experimental groups whenever possible, except in experiments required specific genotypes. |
| Blinding | Researchers were blinded to group allocation during data collection for all animal experiment, by assigning numbers to animals without showing treatment condition. Take experiments on pattern electroretinogram and quantification of optic nerve axons in glaucoma model for example, the person performing the recording or quantification did not know the treatment group of the animal. For cell culture experiment, researchers were not blinded to the treatment condition to avoid any plate mixing. Data analysis was not blinded, as data collected from numbered animals has to be distributed to individual groups. |

# Reporting for specific materials, systems and methods

We require information from authors about some types of materials, experimental systems and methods used in many studies. Here, indicate whether each material, system or method listed is relevant to your study. If you are not sure if a list item applies to your research, read the appropriate section before selecting a response.

## Materials & experimental systems

| n/a | Involved in the study |
|---|---|
| ☐ | ☒ Antibodies |
| ☐ | ☒ Eukaryotic cell lines |
| ☒ | ☐ Palaeontology |
| ☐ | ☒ Animals and other organisms |
| ☒ | ☐ Human research participants |
| ☒ | ☐ Clinical data |

## Methods

| n/a | Involved in the study |
|---|---|
| ☒ | ☐ ChIP-seq |
| ☐ | ☒ Flow cytometry |
| ☒ | ☐ MRI-based neuroimaging |

# Antibodies

| | |
|---|---|
| Antibodies used | Staining: Mouse anti-Oct4 (1:100, BD bioscience 611203), Rabbit anti-Sox2 (1:100, Cell signaling 14962), Goat anti-Klf4 (1:100, R&D system AF3158), Rabbit anti-phosphorylated S6 Ser235/236 (1:100, Cell Signaling 4857), Mouse anti-Brn3a (1:200, EMD Millipore MAB1585), Rabbit anti-Ki67(1:100, Abcam ab15580), Mouse anti-AP2 alpha (1:100, Developmental Studies Hybridoma Bank 3B5), Rabbit anti-pStat3 (Tyr705) (1:100, Cell signaling 9145S), Rat anti-HA (1:400, Roche 11867423001), Rabbit anti-5mC (1:100, Cell signaling 28692S), Rabbit anti-5hmC (1:100, Active Motif 39769), Rat anti-BrdU (1:200, Abcam ab6326), Rabbit anti-Olig2 (1:100, Novusbio NBP1-28667), Chicken anti-GFP (1:10,000, Aves Labs GFP-1020), Guinea pig anti-RBPMS (1:400, Raygene custom order A008712 to peptide GGKAEKENTPSEANLQEEEVRC) and Thy1.2-PE-Cy7 antibody (1:2000, Invitrogen 25-0902-81).<br><br>Western Blot: Rabbit anti-Sox2 (1:100, EMD Millipore, AB5603), Mouse anti-Klf4 (1:1,000, ReproCell, 09-0021), Rabbit anti-p-S6 (S240/244) (1:1,000, CST, 2215), Mouse anti-S6 (1:1,000, CST, 2317), Mouse anti-β-Tubulin (1:1,000, Sigma-Aldrich, 05-661), Mouse anti-β-Actin–Peroxidase antibody (1:20,000, Sigma-Aldrich, A3854). |
| Validation | Mouse anti-Oct4 (1:100, BD bioscience 611203): Mouse and human, Immunofluorescence, validated on manufactures's website: |

https://www.bdbiosciences.com/us/applications/research/stem-cell-research/cancer-research/human/purified-mouse-anti-oct-34-40oct-3/p/611203

Rabbit anti-Sox2 (1:100, Cell signaling 14962), Mouse and human, Immunohistochemistry, validated on manufactures's website: https://www.cellsignal.com/products/primary-antibodies/sox2-d1c7j-xp-rabbit-mab/14962?Ntk=Products&Ntt=14962

Goat anti-Klf4 (1:100, R&D system AF3158), Mouse, Immunohistochemistry, validated on manufactures's website: https://www.rndsystems.com/products/mouse-klf4-antibody_af3158

Rabbit anti-phosphorylated S6 Ser235/236 (1:100, Cell Signaling 4857), Mouse, Immunohistochemistry, validated on manufactures's website: https://www.cellsignal.com/products/primary-antibodies/phospho-s6-ribosomal-protein-ser235-236-91b2-rabbit-mab/4857?Ntk=Products&Ntt=4857

Mouse anti-Brn3a (1:200, EMD Millipore MAB1585), Mouse, Immunohistochemistry, validated on manufactures's website: https://www.emdmillipore.com/US/en/product/Anti-Brn-3a-Antibody-POU-domain-protein-clone-5A3.2,MM_NF-MAB1585

Rabbit anti-Ki67(1:100, Abcam ab15580), Mouse, Immunohistochemistry, validated on manufactures's website: https://www.abcam.com/ki67-antibody-ab15580.html

Mouse anti-AP2 alpha (1:100, Developmental Studies Hybridoma Bank 3B5), Mouse, Immunohistochemistry, validated on manufactures's website: https://www.labome.com/product/Developmental-Studies-Hybridoma-Bank/3B5.html

Rabbit anti-pStat3 (Tyr705) (1:100, Cell signaling 9145S), Mouse, Immunohistochemistry, validated on manufactures's website: https://www.cellsignal.com/products/primary-antibodies/phospho-stat3-tyr705-d3a7-xp-rabbit-mab/9145?Ntk=Products&Ntt=9145

Rat anti-HA (1:400, Roche 11867423001), HA peptide sequence (YPYDVPDYA), immunocytochemistry, validated on manufactures's website: https://www.sigmaaldrich.com/content/dam/sigma-aldrich/docs/Roche/Bulletin/1/roahahabul.pdf

Rabbit anti-5mC (1:100, Cell signaling 28692S), All, Immunohistochemistry, validated on manufactures's website: https://www.cellsignal.com/products/primary-antibodies/5-methylcytosine-5-mc-d3s2z-rabbit-mab/28692?Ntk=Products&Ntt=28692

Rabbit anti-5hmC (1:100, Active Motif 39769), All, Immunohistochemistry, validated on manufactures's website: https://www.activemotif.com/catalog/details/39769.html

Rat anti-BrdU (1:200, Abcam ab6326), Not applicable, Immunohistochemistry, validated on manufactures's website: https://www.abcam.com/brdu-antibody-bu175-icr1-proliferation-marker-ab6326.html

Rabbit anti-Olig2 (1:100, Novusbio NBP1-28667), Mouse, Immunohistochemistry, validated on manufactures's website: https://www.novusbio.com/products/olig2-antibody_nbp1-28667

Chicken anti-GFP (1:10,000, Aves Labs GFP-1020), GFP, Immunohistochemistry, validated on manufactures's website: https://www.aveslabs.com/products/green-fluorescent-protein-gfp-antibody

Guinea pig anti-RBPMS (1:400, Raygene custom order A008712 to peptide GGKAEKENTPSEANLQEEEVRC), Mouse, Immunohistochemistry, validated by co-stained with rabbit anti-RBPMS (Abcam ab194213) and observing co-localization at first layer of inner retina (RGCs).

Thy1.2-PE-Cy7 antibody (1:2000, Invitrogen 25-0902-81), Mouse, FACS, validated on manufactures's website: https://www.thermofisher.com/antibody/product/CD90-2-Thy-1-2-Antibody-clone-53-2-1-Monoclonal/25-0902-82

Rabbit anti-Sox2 (1:100, EMD Millipore, AB5603), Mouse, Western Blotting, validated on manufactures's website: https://www.emdmillipore.com/US/en/product/Anti-Sox2-Antibody,MM_NF-AB5603

Mouse anti-Klf4 (1:1,000, ReproCell, 09-0021), Mouse, Western Blotting, validated by dete ting overexpression of Klf4 in liver samples of  Rosa26-M2rtTA/Col1a1-tetOP-OKS-mCherry mice treated with Doxycycline.

Rabbit anti-p-S6 (S240/244) (1:1,000, CST, 2215), Mouse, Western Blotting, validated on manufactures's website: https://www.cellsignal.com/products/primary-antibodies/phospho-s6-ribosomal-protein-ser240-244-antibody/2215?Ntk=Products&Ntt=2215&N=4294960393&Nrpp=100&fromPage=plp

Mouse anti-S6 (1:1,000, CST, 2317), Mouse, Western Blotting, validated on manufactures's website: https://www.cellsignal.com/products/primary-antibodies/s6-ribosomal-protein-54d2-mouse-mab/2317?Ntk=Products&Ntt=2317

Mouse anti-β-Tubulin (1:1,000, Sigma-Aldrich, 05-661), Mouse, Western Blotting, validated on manufactures's website: https://www.sigmaaldrich.com/catalog/product/mm/05661?lang=en&region=US

Mouse anti-β-Actin–Peroxidase antibody (1:20,000, Sigma-Aldrich, A3854), Mouse, Western Blotting, validated on manufactures's website: https://www.sigmaaldrich.com/catalog/product/sigma/a3854?lang=en&region=US

## Eukaryotic cell lines

Policy information about cell lines

| | |
|---|---|
| Cell line source(s) | Ear fibroblasts (EFs) were isolated from Reprogramming 4F (Jackson Laboratory 011011) or 3F (Hochedlinger lab, Harvard) mice. SH-SY5Y neuroblastoma cells were obtained from the American Tissue Culture Collection (ATCC, CRL-2266) and maintained according to ATCC recommendations. |
| Authentication | Primary ear fibroblasts were authenticated using genotyping and qPCR.<br>SH-SY5Y (ATCC CRL-2266) was authenticated using RNA-seq. |
| Mycoplasma contamination | All cell lines were tested routinely and confirmed negative for mycoplasma contamination. |
| Commonly misidentified lines<br>(See ICLAC register) | No commonly misidentified lines were used in this study |

## Animals and other organisms

Policy information about studies involving animals; ARRIVE guidelines recommended for reporting animal research

| | |
|---|---|
| Laboratory animals | For optic nerve crush and glaucoma model experiments, C57BL6/J wild type mice were purchased from the Jackson Laboratory (000664). For ageing experiments, young and old females from the NIA Aged Rodent Colonies were used. Rosa26-M2rtTA/ Col1a1-tetOP-OKS-mCherry alleles were a gift from the Hochedlinger lab (Harvard). Rosa-CAG-lox-STOP-lox-Tomato mice were provided by Fan Wang (Duke). Vglut2-IRES-Cre (016963), Vgat-IRES-Cre (016962), Tet2flox/flox (017573) and Rosa26-M2rtTA/ Col1a1-tetOP-OSKM (011011) were purchased from the Jackson Laboratory. All animal work was approved by the Institutional Animal Care and Use Committees (IACUCs) at Harvard Medical School, Boston Children's Hospital, and the Mass Eye and Ear Institution. Animals were housed under 12-hour light/dark cycles 6am-6pm-6am, 70-72°F ambient temperature, and 40-50% humidity. |
| Wild animals | No wild animals were used in the study. |
| Field-collected samples | No field collected samples were used in the study. |
| Ethics oversight | All animal work was approved by the Institutional Animal Care and Use Committees (IACUCs) at Harvard Medical School, Boston Children's Hospital, and the Mass Eye and Ear Institution. |

Note that full information on the approval of the study protocol must also be provided in the manuscript.

## Flow Cytometry

### Plots

Confirm that:

☒ The axis labels state the marker and fluorochrome used (e.g. CD4-FITC).

☒ The axis scales are clearly visible. Include numbers along axes only for bottom left plot of group (a 'group' is an analysis of identical markers).

☒ All plots are contour plots with outliers or pseudocolor plots.

☒ A numerical value for number of cells or percentage (with statistics) is provided.

### Methodology

| | |
|---|---|
| Sample preparation | For Extended data Fig. 8c, SH-SY5Y neuroblastoma cells were obtained from the American Tissue Culture Collection (ATCC, CRL-2266) and maintained according to ATCC recommendations. SH-SY5Y cells were differentiated into neurons and transduced with corresponding AAV.DJ vectors to allow OSK to express for five days. Cells were then harvested and fixed with 70% cold ethanol for 16 hours at 4°C. After fixation, cells were washed twice with PBS and incubated with PBS containing 50 ug/mL propidium iodide (Biotium, 40017) and 100 ug/mL RNase A (Omega) for 1 hour at room temperature. PI-stained samples were then analyzed. |
| Instrument | BD Biosciences, LSR-II cell analyzer |
| Software | FCS Express 6 |
| Cell population abundance | The nucleated cells (propidium iodide positive) were gated to get ride of debris, and only single cells (but not doublets and larger aggregates) were selected for cell cycle analysis. The single cells are 85%-97% of all nucleated cells across all samples. |

Gating strategy

FSC/SSC profiles were used to exclude debris. Since nucleated cells were later gated based on propidium iodide signal, FSC/SSC gating include more than 95% of the whole cell population to include as many cells/debris as possible. The boundaries between positive and negative propidium iodide staining is clear-cut since propidium iodide is very specific to DNA. The nucleated (propidium iodide positive) cells were gated and scattered on PI-A and PI-W plots and only single cells were gated for cell cycle analysis. G1, S, and G2 gating was determined by FCS Express 6 software and verified by the investigator.

☒ Tick this box to confirm that a figure exemplifying the gating strategy is provided in the Supplementary Information.